Systematic characterization of *Ustilago maydis* sirtuins shows Sir2 as a modulator of pathogenic gene expression

Blanca Navarrete, José I. Ibeas†*, Ramón R. Barrales†*

Centro Andaluz de Biología del Desarrollo (CABD), Universidad Pablo de Olavide-CSIC-Junta de Andalucía, Seville, Spain

† These authors share senior authorship

*** Correspondence:**
Corresponding Author
joibecor@upo.es, rrambar@upo.es

Keywords: Sirtuins, phytopathogenesis, HDAC, histone deacetylases, gene regulation, plant infection, filamentation.

Abstract

Phytopathogenic fungi must adapt to the different environmental conditions found during infection and avoid the immune response of the plant. For these adaptations, fungi must tightly control gene expression, allowing sequential changes in transcriptional programs. In addition to transcription factors, chromatin modification is used by eukaryotic cells as a different layer of transcriptional control. Specifically, the acetylation of histones is one of the chromatin modifications with a strong impact on gene expression. Hyperacetylated regions usually correlate with high transcription and hypoacetylated areas with low transcription. Thus, histone deacetylases (HDACs) commonly act as repressors of transcription. One member of the family of HDACs is represented by sirtuins, which are deacetylases dependent on NAD+, and, thus, their activity is considered to be related to the physiological stage of the cells. This property makes sirtuins good regulators during environmental changes. However, only a few examples exist, and with differences in the extent of the implication of the role of sirtuins during fungal phytopathogenesis. In this work, we have performed a systematic study of sirtuins in the maize pathogen *Ustilago maydis*, finding Sir2 to be involved in the dimorphic switch from yeast cell to filament and pathogenic development. Specifically, the deletion of *sir2* promotes filamentation, whereas its overexpression highly reduces tumor formation in the plant. Moreover, transcriptomic analysis revealed that Sir2 represses genes that are expressed during biotrophism development. Interestingly, our results suggest that this repressive effect is not through histone deacetylation, indicating a different target of Sir2 in this fungus.

Introduction

Phytopathogenic fungi must sense many environmental host cues and respond with developmental changes in order to ensure proper plant infection progression. In the well-established model organism *Ustilago maydis*, a biotrophic pathogen infecting maize plants, the first step in the pathogenic program is the switch from yeast to filament on the surface of the plant, followed by the fusion of two sexually compatible filaments. This dikaryotic filament blocks the cell cycle and extends until it identifies the appropriate location for penetration, where it develops a specialized invasive structure, the appressoria. Upon plant penetration, the filament releases the cell cycle block and colonizes the plant until the development of teliospores inside plant tumors induced by the fungus (Brefort et al., 2009; Vollmeister

et al., 2012; Castanheira and Pérez-Martín, 2015). All these sequential changes must be tightly controlled in order to ensure successful infection. Many advances have been achieved in determining the transcription factors involved in this control mechanism in many fungi. In *U. maydis*, environmental cues are transmitted by the MAP kinases and cAMP signaling pathways to the Prf1 transcription factor, which controls, among others, the bE/bW compatible heterodimer transcribed from the MAT b locus in the dikaryon. This heterodimer controls many downstream virulence genes, including other important transcription factors (Hartmann et al., 1996, Hartman et al., 1999; Brachmann et al., 2001; Heimel et al., 2010; Lanver et al., 2017).

Another layer of control is chromatin modification, which plays crucial roles in transcriptional regulation in response to environmental cues (Mazzio and Soliman, 2012; Rando and Winston, 2012; Badeaux and Shi, 2013). Histone modifiers carry out different posttranslational modifications in the histone tails, such as acetylation, methylation or phosphorylation, among others, with potential alterations in the transcriptional stages of the surrounding area. One of the major and most well-described histone modifications, together with methylation, is the acetylation in a lysine residue (Allfrey et al., 1964). The enzymes responsible for this acetylation are called histone acetyltransferases (HATs), and those involved in the removal of this modification are the histone deacetylases (HDACs).

The role of these chromatin modifiers in pathogenesis has been explored in different fungi. Gcn5 is the main HAT studied in plant pathogenic fungi, with important roles in development and infection (Ruijter et al., 2003; González-Prieto et al., 2014; Kong et al., 2018; Liu et al., 2022). In *U. maydis*, the deletion of Gcn5 causes constitutive filamentation and reduction of infection by, at least, the derepression of *prf1* and *bE1* genes (González-Prieto et al., 2014). On the other hand, the roles of HDACs during fungal plant pathogenesis, although poorly characterized, are better known than those for HATs. HDACs can be classified into three main different categories, Class I, II and III, based on their homology to the yeast orthologues Rpd3, Hda1 and Sir2, respectively (Ruijter et al., 2003). Among Class I/II HDACs, the Set3 complex, comprising the HDAC Hos2, is one of the best studied in fungal plant pathogens, with conserved roles in pathogenesis (Elías-Villalobos et al., 2019). In *U. maydis*, Hos2 affects filamentation and pathogenesis through direct regulation of the MAT a locus (Elías-Villalobos et al., 2015). In addition to Hos2, other Class I/II HDACs, Hda1 and Hda2, have also been characterized in *U. maydis*. Hda1 is essential for teliospore production with a role in gene regulation, repressing the transcription of *egl1* and *mig1* during the non-pathogenic state of the fungus (Reichmann et al., 2002; Torreblanca et al., 2003). In contrast, deletion of *hda2* did not alter the infection capability of *U. maydis*. (González-Prieto et al., 2004; Elías-Villalobos et al., 2015). Class III HDACs constitute a particular group of histone deacetylases that are dependent on NAD^+ for their catalytic activity (Tanner et al., 2000; Tanny and Moazed, 2001; Jackson and Denu, 2002; Zhao and Rusche, 2022). The founding member of this class, collectively named sirtuins, is Sir2 (Silent Information Regulator 2) from *Saccharomyces cerevisiae*. ScSir2 forms a complex with other SIR proteins and is involved in the silencing of heterochromatin-like regions in this yeast by deacetylating H4 lysine 16 residue (H4K16) (Robyr et al., 2002; Suka et al., 2002). The role of Sir2 in chromatin silencing is broadly observed, with examples also described in filamentous fungi, such as *Neurospora crassa* or *Aspergillus nidulans* (Smith et al., 2008; Shimizu et al., 2012; Itoh et al., 2017), which suggests an ancient role of this protein in silencing (Hickman et al., 2011). In addition to Sir2, other sirtuins have been characterized in different organisms. In *S. cerevisiae* and *Schizosaccharomyces pombe*, all the other sirtuins, Hst1 to 4 in *S. cerevisiae* and Hst2 and 4 in *S. pombe*, have been linked to chromatin silencing as well as direct gene regulation (Brachmann et al., 1995; Freeman-Cook et al., 1999; Sutton et al., 2001; Halme et al., 2004; Wilkins et al., 2014). Within the sirtuin family, Sir2 has been described to control pathogenesis in different fungi. For instance, in the human pathogen *Candida glabrata*, Sir2 represses the EPA adhesin genes, which are essential for infection (Domergue et al.,

85 2005), and in *Cryptococcus neoformans*, Sir2 is essential for virulence, due to a mechanism not
86 described so far (Arras et al., 2017). The main example to date for the role of Sir2 in plant pathogens
87 is found in *Magnaporthe oryzae*. In this rice pathogen, Sir2 likely affects infection through inactivation
88 by deacetylation of the MoJmjC repressor, which would lead to an increase in superoxide dismutase
89 expression, allowing ROS detoxification (Fernandez et al., 2014).

90 In order to increase our knowledge regarding the role of sirtuins in fungal plant pathogens, we have
91 performed a characterization of the sirtuin family in *U. maydis*. We have observed that two of the five
92 sirtuins present in *U. maydis*, Sir2 and Hst4, display nuclear localization during the entire cell cycle.
93 From them, Hst4 is essential and Sir2 negatively impacts the yeast to filament transition and virulence.
94 While the deletion of *sir2* slightly increases the virulence capacity, its overexpression significantly
95 reduces virulence. A transcriptomic analysis of both deletion in filamentation conditions and
96 overexpression during infection indicates that Sir2 avoids the proper activation of a group of genes
97 induced during the biotrophic development. We have observed an increase in H4 acetylation in a Δ*sir2*
98 mutant in the upregulated genes. However, this deacetylation is not detected in the typical residue
99 observed in other organisms, lysine 16. As these effects may be the consequence of the increase in
100 transcription observed, further analyses are required in order to detect the specific target of Sir2 in
101 terms of its regulatory role in *U. maydis*.

102 **Materials and Methods**

103 **Strains and growth condition**

104 *Escherichia coli* DH5α, pJET1.2/blunt (Thermo Scientific, Carlsbad, CA, USA) and pBluescript II SK
105 (+) (Stratagene, San Diego, CA, USA) were used for cloning purposes. The growth conditions for *E.*
106 *coli* were described in (Sambrook et al., 1989). All the strains used in this study are derived from the
107 haploid pathogenic SG200 strain and are listed in Supplementary Table S1. As previously described in
108 (Gillissen et al., 1992), *U. maydis* cultures were performed in YEPSL (0.4% bactopeptone, 1% yeast
109 extract and 0.4% saccharose) at 28ºC, unless otherwise specified. For charcoal filamentation assays,
110 exponential cultures were spotted onto PD–charcoal plates (2.4% potato dextrose broth, 1% charcoal,
111 2% agar) and grown for 18-20 hours at 25ºC. Pathogenicity assays were performed as described in
112 (Kämper et al., 2006). *U. maydis* exponential cultures were concentrated to an OD_{600} of 0.5 or 1 and
113 injected into 7-day-old maize (*Zea mays*) seedlings (Early Golden Bantam). Disease symptoms were
114 quantified at 14 dpi. Data of individual infection experiments are listed in Supplementary Table S2.
115 Statistical analyses were performed in the GraphPad Prism 8 software.

116 **Plasmid and strain construction**

117 Molecular biology techniques were used, as previously described (Sambrook et al., 1989). *U. maydis*
118 DNA isolation and transformation procedures were carried out following the protocol described in
119 (Schulz et al., 1990). Deletion mutants for *sir2* (UMAG_00963), *hst2* (UMAG_05892), *hst4*
120 (UMAG_05758) and *hst5* (UMAG_05239) were generated by homologous recombination, as
121 described previously (Brachmann et al., 2004; Kämper, 2004). Deletion for *hst6* (UMAG_12006) was
122 performed using the NEBuilder HiFi DNA Assembly (New England Biolabs, Ipswich, MA, USA)
123 system. The *sir2* complementation mutant was generated by reintroducing the *sir2* open reading frame
124 (ORF) in the Δ*sir2* background in its endogenous loci, replacing the nat resistance cassette of the Δ*sir2*
125 mutant with the *sir2* ORF, followed by the geneticin resistance cassette by homologous recombination.
126 For *sir2* overexpression with the *otef* promoter, the p123-P*otef*:*sir2* plasmid was generated by replacing
127 the eGFP fragment from the p123 plasmid (Aichinger et al., 2003) with the *sir2* ORF. The *sir2* ORF
128 was amplified by PCR using Q5 High-Fidelity DNA polymerase (New England Biolabs, Ipswich, MA,

129 USA) and cloned into p123 within the NcoI and NotI restriction sites of p123. For *sir2* overexpression
130 with the *pit2* promoter, we constructed the p123-P*pit2*:*sir2* plasmid. The *sir2* ORF was amplified and
131 cloned into p123-P*pit2* within the NcoI and XbaI restriction sites of p123-P*pit2*. To generate SG200
132 P*otef*:*sir2* or SG200 P*pit2*:*sir2*, p123-P*otef*:*sir2* or p123-P*pit2*:*sir2* was linearized with SspI and
133 integrated into the *ip* locus by homologous recombination. For GFP endogenous sirtuin tagging, the
134 plasmids pBSK-*sir2*:eGFP, pBSK-*hst2*:eGFP, pBSK-*hst4*:eGFP, pBSK-*hst5*:eGFP and pBSK-
135 *hst6*:eGFP were generated using the NEBuilder HiFi DNA Assembly (New England Biolabs, Ipswich,
136 MA, USA) system. A 1 Kb fragment containing the gene of interest (ORF without the STOP codon)
137 and a 1 Kb fragment of the 3' region were amplified using primers designed in the NEBuilder assembly
138 tool. eGFP followed by hygromycin resistance cassettes were amplified from the pmf5-1h plasmid
139 (Becht et al., 2006). All the fragments were cloned into the pBluescript II SK (+) plasmid using the
140 NEBuilder HiFi DNA Assembly (New England Biolabs, Ipswich, MA, USA). Constructs were
141 amplified by PCR prior to their transformation in *U. maydis.* The primers used in this study are listed
142 in Supplementary Table S3. All the strains and numbers of copies integrated into the *ip* locus were
143 verified by PCR and Southern blotting.

144 **Microscopy and image analysis**

145 To analyze the filamentation capability of *U. maydis* in PD-charcoal plates, single colonies where
146 visualized using the Leica M205 Stereoscope equipped with an ORCA-Flash4.0 LT Hamamatsu digital
147 camera. The area of the colonies was measured by selecting the perimeter of each colony using the
148 plugging convex hull of ImageJ software. To determine sirtuins' localization, *sir2*:eGFP, *hst2*:eGFP,
149 *hst4*:eGFP, *hst5*:eGFP and *hst6*:eGFP cells were visualized using a DeltaVision microscopy system
150 comprising an Olympus IX71 microscope and CoolSnap HQ camera (Applied Precision, Issaquah WA,
151 USA). To visualize mitochondria, 0.5 mM Mito-Tracker CM-H2Xros (Molecular Probes, Eugene, OR)
152 was added to the *U. maydis* YEPSL cell culture and cells were incubated for 15 min at 25ºC (Bortfeld
153 et al., 2004). To analyze the *U. maydis* progression inside the maize plant, leaves samples from 3, 4
154 and 6 dpi infected plants were distained with ethanol, treated for 4 h at 60ºC with 10% KOH, washed
155 in phosphate buffer and then stained with propidium iodide (PI) to visualize plant tissues in red and
156 wheat germ agglutinin (WGA)/AF488 to visualize the fungus in green. At least four leaves from two
157 independent experiments were stained and visualized by fluorescence microscopy (Leica SPE
158 DM2500, Leica, WZ, Germany). Image processing was carried out using the ImageJ software.

159 **RNA extraction and RT-qPCR**

160 Total RNA was extracted from *U. maydis* cells grown in YEPSL medium, PD–charcoal plates and
161 from infected leaves by excising 2–3 cm segments from below the injection holes. All the samples
162 were ground into a powder using a mortar/pestle under liquid nitrogen. Total RNA was purified using
163 TRIzol reagent (Invitrogen, Carlsbad, CA, USA) and the Direct-zol RNA Miniprep Plus Kit (Zymo
164 Research, Irvine, CA, USA). RNA was retrotranscribed from 3 µg of total RNA using the RevertAid
165 H Minus First Strand cDNA Synthesis Kit (Thermo Scientific, Carlsbad, CA, USA). RT-qPCR was
166 performed using a Real-Time CFX Connect (Bio-Rad, Hercules, CA, USA) and SYBR Premix Ex Taq
167 II (Tli RNase H Plus) (Takara Bio INC, Kusatsu, Japan). All reactions were performed in at least three
168 biological replicates, and gene expression levels were calculated relative to the expression levels of the
169 constitutively expressed fungal *ppi1* gene. Primers used for RT-qPCR are listed in Supplementary
170 Table S2. The quantification of relative fungal biomass in infected maize leaves was performed as
171 previously described (Brefort et al., 2014). *U. maydis* biomass was quantified measuring the signal of
172 the *ppi1* fungal gene relative to the plant gene GAPDH. Statistical analyses were performed in the
173 GraphPad Prism 8 software.

174 **RNA-Seq analysis**

175 Total RNA extracted from axenic cultures and PD–charcoal plates from *U. maydis* wild-type and Δ*sir2*
176 strains was submitted to BGI TECH SOLUTIONS (HONGKONG) CO., LIMITED, in a 200-500 ng/µl
177 concentration, with a total RNA quantity of 5 - 8 µg and quality parameters of $OD_{260/280}$ = 1.8-2.1 and
178 $OD_{260/230}$ > 1.5. The BGI company prepared all libraries and performed the single-end sequencing via
179 the BGISEQ-500 RNA-Seq service. Two replicates of each strain and condition were processed. To
180 determine Sir2-regulated genes during pathogenesis, 7-day-old maize seedlings were infected with
181 wild-type and P*pit2*:*sir2* >1c strains and total RNA was purified at 3 dpi. RNA samples were submitted
182 to BGI TECH SOLUTIONS (HONGKONG) CO., LIMITED, and paired-end sequenced via the
183 DNBseq PE100 service. Three replicates of each strain were processed. Reads were mapped to the *U.*
184 *maydis* genome using HISAT2 and reads from infected plant tissues were previously filtered against
185 the annotated maize genome. Reads were counted for *U. maydis* using the HTseq tool in the Galaxy
186 platform, and, for expression analysis, only uniquely mapping exon read counts were considered.
187 Pairwise comparisons were performed using the R package DESeq2 (Love et al., 2014). Genes with
188 log2 fold change > 0.5 or <-0.5 and adjusted p-value < 0.05 were considered differentially regulated.

189 **Western blot analysis**

190 For total protein extraction, cells from exponential culture were collected by centrifugation and washed
191 twice with 20 mM Tris–HCl pH 8.8. Pellets were ground to powder with a mortar under liquid nitrogen
192 and resuspended in RIPA buffer (50 mM Tris–HCl, pH 8, 150 mM NaCl, 1% Nonidet P-40, 0.5%
193 sodium deoxycholate, 0.1% SDS) supplemented with 1 µg/ml Pepstatin A (PanReac AppliChem,
194 Barcelona, Spain), 1 µg/ml Bestatin (Thermo Scientific, Carlsbad, CA, USA), 1mM PMSF (PanReac
195 AppliChem, Barcelona, Spain) and EDTA-free protease inhibitor complex (cOmplete Tablets EDTA-
196 free, Roche, Mannheim, BW, Germany). After cell lysis, samples were centrifuged and the supernatant
197 was collected. For protein extraction in PD–charcoal plates, cells were scraped off and ground to
198 powder in liquid nitrogen and resuspended in 12% TCA solution to precipitate proteins. Pellets were
199 washed 4 times with ice-cold acetone and dissolved in extraction buffer (100 mM Tris–HCl pH 8, 50
200 mM NaCl, 1% SDS, 1mM EDTA) supplemented with the protease inhibitors listed above. Protein
201 concentration was measured by the BCA protein assay. Here, 40 µg of protein extract was loaded into
202 a 10% TGX Stain-Free FastCast Acrylamide Gel (Bio-Rad, Hercules, CA, USA) or SDS
203 polyacrylamide 15% running gel in the case of histone analysis. Separated proteins were transferred
204 into a nitrocellulose membrane using the Trans-Blot Turbo transfer system (Bio-Rad, Hercules, CA,
205 USA). The membrane was incubated with mouse polyclonal anti-GFP antibody (Roche, Mannheim,
206 BW, Germany) (1:1000 in PBST 5% fat-free milk) and anti-mouse IgG HRP conjugated (Invitrogen,
207 Carlsbad, CA, USA) (1:5000) was used as a secondary antibody. Histone modifications were detected
208 with primary antibodies specific to H3 (Sigma-Aldrich, Darmstadt, Germany), H3ac (Sigma-Aldrich,
209 DA, Germany), H3K9ac (abcam, Cambridge, UK) (1:5000 in PBST 5% fat-free milk), H4 (Sigma-
210 Aldrich, Darmstadt, Germany), H4ac (Sigma-Aldrich, Darmstadt, Germany) (1:5000 in PBST 3%
211 BSA) and H4K16ac (Sigma-Aldrich, Darmstadt, Germany) (1:5000 in PBST 5% fat-free milk) and
212 anti-rabbit HRP conjugated as a secondary antibody (Sigma-Aldrich, Darmstadt, Germany) (1:5000).
213 Chemiluminescence was detected with SuperSignal™ West Femto Maximum Sensitivity Substrate
214 (Thermo Scientific, Carlsbad, CA, USA). Image gel and membrane acquisition was carried out with
215 the ChemiDoc XRS (Bio-Rad, Hercules, CA, USA). All the Western blot assays were performed with
216 at least three biological replicates and quantified using the Image Lab software.

217

218

219 **Chromatin Immunoprecipitation (ChIP)**

220 Exponential culture of *U. maydis* cells were cross-linked by incubating with 1% formaldehyde for 10
221 minutes and reaction stopped by adding glycine to a final concentration of 250 mM for 10 minutes at
222 room temperature. Cells were collected by centrifugation and washed twice with cold PBS. 2x 250 mg
223 of pellets were ground to powder with a mortar under liquid nitrogen and resuspended in ChIP lysis
224 Buffer (50 mM HEPES-KOH pH 7.5, 140 mM NaCl, 1 mM EDTA pH 8, 1% Triton X-100, 0.1% Na-
225 deoxycholate, 0.1% SDS) supplemented with 1 µg/ml Pepstatin A (PanReac AppliChem, Barcelona,
226 Spain), 1 µg/ml Bestatin (Thermo Scientific, Carlsbad, CA, USA), 1mM PMSF (PanReac AppliChem,
227 Barcelona, Spain) and EDTA-free protease inhibitor complex (cOmplete Tablets EDTA-free, Roche,
228 Mannheim, BW, Germany). Samples were then sonicated in a Bioruptor® sonication device
229 (Diagenode) for 20 min, with 2 minutes pulses separated by 1 minute rest periods at maximum power.
230 100 µl of the chromatin extract was kept as input and a total of 10 O.D. of chromatin extract was used
231 for IP. Samples were incubated with 3 µl of antibodies against H3ac (Sigma-Aldrich, DA, Germany),
232 H4 (Sigma-Aldrich, Darmstadt, Germany), H4ac (Sigma-Aldrich, Darmstadt, Germany) and H4K16ac
233 (Sigma-Aldrich, Darmstadt, Germany) at 4°C overnight on a rotary shaker. Precipitation of the protein-
234 antibody conjugate was performed incubating with Dynabeads® Protein A (Thermo Scientific,
235 Carlsbad, CA, USA) 40 minutes at 4ºC in a rotary shaker. Beads were washed twice with WB150 (20
236 mM Tris-HCl pH 8, 150 mM NaCl, 2 mM EDTA pH 8, 1% Triton X-100), once with WB500 (20 mM
237 Tris-HCl pH 8, 500 mM NaCl, 2 mM EDTA pH 8, 1% Triton X-100) and eluted in TES buffer (50
238 mM Tris-HCl pH 8, 10 mM EDTA, 1% SDS). To reverse the crosslink, both input and IP chromatin
239 extracts were incubated at 65°C for 16 hours. Histone-bound DNA was treated with Proteinase K
240 (Thermo Scientific, Carlsbad, CA, USA) and DNA purification was done using the ChIP DNA Clean
241 & Concentrator™ (Zymo Research, Irvine, CA, USA). For RT-qPCR a 20-fold dilution of each
242 immunoprecipitated sample and a 200-fold dilution of input samples were used. Primers used for each
243 amplicon were listed in Supplementary Table S2. All experiments were performed with three biological
244 replicates.

245 **Results**

246 **The systematic characterization of sirtuins in *U. maydis* shows Sir2 as a nuclear sirtuin**
247 **controlling cell-to-filament transition**

248 In a previous phylogenetic analysis (Elías-Villalobos et al., 2019), five sirtuin homologs were described
249 in *U. maydis*: UMAG_00963 (Sir2), UMAG_05892 (Hst2), UMAG_05758 (Hst4), UMAG_05239
250 (Hst5) and UMAG_12006 (Hst6). As expected, all these proteins contained the conserved sirtuin
251 catalytic domain (PROSITE:PS50305) involved in protein deacetylation (Figure 1A). Additionally, we
252 detected nuclear localization signals in only Sir2 and Hst4 (Figure 1A). As we were interested in
253 studying the possible role of sirtuins in the control of the transcriptional pathogenic program, we
254 examined the cellular localization of these proteins in order to focus on the nuclear ones. Consistent
255 with their localization motifs, we observed that Sir2 and Hst4 displayed nuclear localization (Figure
256 1B). Additionally, Hst2 showed a nuclear signal only in mitotic cells (Figure 1B). By contrast, Hst5
257 and 6 were localized in the mitochondria, as verified by Mito-tracker colocalization (Figure 1B and
258 Supplementary Figure S1A). This is consistent with the similarity described for these sirtuins to
259 mitochondrial ones (Elías-Villalobos et al., 2019). In addition to the cellular localization study, we
260 deleted all sirtuin genes in the solopathogenic strain SG200, except for the *hst4* gene, whose deletion
261 we found to be lethal (Supplementary Figure S2B). We performed plant infection assays with these
262 mutants and found no significant changes in the symptoms of plants infected with Δ*hst2,* Δ*hst5* or
263 Δ*hst6* mutants compared to the wild-type strain (Supplementary Figure S1C). However, we detected a

264 slight increase in the symptoms of plants infected with the Δ*sir2* mutant (Figure 1C). A more significant
265 difference was observed when we studied the yeast to filament transition in solid PD–charcoal plates,
266 which mimicked the hydrophobic conditions of the plant surface. Here, we observed an increase in the
267 filamentation capability of the Δ*sir2* mutant (Figure 1D and Supplementary Figure S1D), which was
268 restored to its normal level after the reintroduction of *sir2* in the endogenous locus (Supplementary
269 Figure S1D). We quantified this increase in filamentation by growing individual colonies on PD-
270 charcoal plates and measuring filaments length of the single colonies, observing that Δ*sir2* colonies
271 exhibit longer filaments compared to wild-type (Figure 1D). No changes in filamentation were
272 observed for the rest of the sirtuin mutants (Supplementary Figure S1D).

273 **Sir2 affects the transcription of some genes during filamentation**

274 In order to disregard a possible pleiotropic effect of *sir2* deletion, we performed growth assays in rich
275 (YEPSL), complete (CMD) and minimal (MMD) media (Supplementary Figure S2A), flow cytometry
276 analysis of DNA-stained cells (Supplementary Figure S2B) and a stress assay with sorbitol and NaCl
277 as osmotic stressors, H_2O_2 as an oxidant, SDS as a membrane-perturbing drug, calcofluor white (CFW)
278 and Congo red as cell wall integrity sensors and Tunicamycin and DTT as endoplasmic reticulum
279 stressors (Supplementary Figure S2C). We were not able to detect any significant differences with
280 respect to wild-type cells, suggesting no pleiotropy. Thus, we focused on the role of Sir2 in cell to
281 filament transition. We analyzed Sir2 protein levels and observed a drastic reduction in Sir2 during
282 filamentation (Figure 2A). Although Sir2 is mainly present in axenic conditions, and its deletion caused
283 an increase in filamentation on PD–charcoal plates, no filaments were found in the Δ*sir2* mutant in
284 axenic conditions (Figure 2B). In addition, almost no differences in gene expression were found by
285 RNA sequencing (RNA-seq) analysis in a Δ*sir2* mutant in axenic conditions (Figure 2C and
286 Supplementary Table S4). The most upregulated gene was *eff1-9* (Figure 2C and Supplementary Table
287 S4), a member of the *eff* family of effector proteins important for virulence (Khrunyk et al., 2010;
288 Schuster et al., 2018). *eff1-9* upregulation was confirmed by RT-qPCR in the Δ*sir2* mutant and the
289 transcription levels were restored in the complementation strain (Supplementary Figure S2D). The
290 other upregulated genes were two subtelomeric genes, UMAG_04104 and UMAG_05781, and three
291 genes involved in metabolism, UMAG_01476, UMAG_04922 and UMAG_01656 (Figure 2C and
292 Supplementary Table S4). We then analyzed transcription changes in a Δ*sir2* mutant in filament-
293 induced PD–charcoal plates by RNA-seq. We obtained 11 downregulated and 31 upregulated genes
294 (Figure 2D and Supplementary Table S5). Many of the upregulated genes, 58%, encoded for predicted
295 effector proteins, including many of the previously characterized ones: Mig2-6 (Farfsing et al., 2005),
296 Pit1 and 2 (Doehlemann et al., 2011; Mueller et al., 2013), Eff1-7 (Khrunyk et al., 2010), Cmu1
297 (Djamei et al., 2011), Rsp3 (Ma et al., 2018), Erc1 (Ökmen et al., 2022) and Egl1 and 3 (Schauwecker
298 et al., 1995; Doehlemann et al., 2008). In order to know if the Δ*sir2* upregulated genes are genes which
299 have to be expressed when filamentation is induced in PD-charcoal plates, we studied the distribution
300 of the significantly different log2 fold changes in expression of all these genes during charcoal growth,
301 in comparison with axenic conditions, in a wild-type strain (Supplementary Table S6). We observed
302 that when all genes of a wild-type strain were analyzed, there was a general distribution in which log2
303 fold changes expanded from negative to positive values (Figure 2E). However, the group of genes that
304 were upregulated in Δ*sir2* corresponded to genes upregulated during charcoal growth (Figure 2E,
305 Supplementary Table S5 and Supplementary Table S6). As comparison between growth on charcoal
306 plates versus liquid rich media imply other changes different than filamentation, we crossed our data
307 with other datasets more specific for filamentation. Interestingly, we found that 42% of the upregulated
308 genes in the Δ*sir2* mutant are genes upregulated when filamentation and appressoria formation is
309 induced by an hydrophobic surface and hydroxy fatty acids (Lanver et al., 2014) (Supplementary Table
310 S5). Interestingly, *egl1* has been previously identified as a gene specifically expressed in filaments

311 (Schauwecker et al., 1995). As many of the described effectors found to be upregulated in a Δ*sir2*
312 mutant have their effect during infection, we also studied the possibility of these genes being activated
313 during the infection process. In a previous study of the transcriptional changes observed during
314 infection performed by RNA-seq, Lanver *et al*., 2018 (Lanver et al., 2018) described different modules
315 of coexpressed genes during infection. We observed the strong enrichment of genes belonging to the
316 cyan (26%) and the magenta (52%) modules in the group of genes upregulated in Δ*sir2* in comparison
317 to all the upregulated genes during filamentation (Figure 2F Supplementary Table S5 and
318 Supplementary Table S6). The magenta module correlates with the establishment and maintenance of
319 biotrophy, while the cyan one represents a tumor module (Lanver et al., 2018). All these data may
320 indicate a role of Sir2 in avoiding the proper activation of a group of genes induced during filamentation
321 and probably during infection.

322 **Sir2 overexpression drastically reduces infection capability**

323 The observation that Sir2 affects the expression of genes that are induced during infection led us to
324 study the role of Sir2 during plant infection. As the deletion of *sir2* showed a slight increase in infected
325 plant symptoms (Figure 1C), and Sir2 seemed to repress genes activated during infection (Figure 2F),
326 we decided to study the effect of *sir2* overexpression. First, we integrated one or more than one copy
327 of the *sir2* gene under the control of the constitutive *otef* promoter in the *ip* locus. No growth defects
328 were detected in the overexpression mutant (Supplementary Figure S3A), however, as it can be
329 observed in Figures 3A, B and Supplementary Figure S3C, the filamentation capability was reduced
330 according to the *sir2* expression level found in both mutants. These data confirm the role of Sir2 in
331 avoiding the proper induction of the filamentation process. Additionally, we overexpressed *sir2* during
332 pathogenesis by using the *pit2* promoter, which reaches its expression peak at 2 days post-infection
333 (dpi) (Figure 4C). We infected maize plants with mutants harboring one or more than one copy of
334 *Ppit2:sir2*, which did not show any significant defect in growth in different tested media
335 (Supplementary Figure S3B), and quantified the symptoms in infected plants. The size of tumors was
336 clearly reduced when *sir2* was significantly induced at 3 dpi (Figures 3C, D), indicating that Sir2 affects
337 the infection process during plant colonization. When we analyzed the pathogenic defects of this
338 mutant, we did not detect any alteration in fungi morphology during plant colonization (Figure 4A).
339 However, after 3 dpi, we detected a gradual reduction in fungal biomass during the progression of
340 infection (Figure 4B). It is interesting to note that the reduction in fungal biomass was detected several
341 days after the main overexpression of *sir2*, obtained at 2 dpi (Figure 4C). A possible explanation is that
342 the overexpression of *sir2* during the biotrophy establishment (2 dpi), affects the transcription of
343 effector genes essential for this process or genes with roles from 4 dpi onward. Another alternative
344 may be that the reduction in biomass observed (Figure 4B) is through an expression-independent effect
345 of Sir2.

346 **Sir2 prevents induction of a pool of virulence genes**

347 To study the effect of Sir2 overexpression on gene transcription during infection, we carried out RNA-
348 seq analysis of maize leaves infected with the wild-type strain or the mutant with more than one copy
349 of P*pit2*:*sir2* at 3 dpi, when there was no significant change in fungal biomass and *sir2* had been highly
350 induced. We identified 51 genes downregulated and 39 upregulated in the mutant compared to the
351 wild-type strain (Figure 5A and Supplementary Table S7), with the downregulated genes showing a
352 stronger change in terms of differential expression. When we considered the distribution of
353 transcriptional fold changes in a wild-type strain at 3 days post-infection in comparison to axenic
354 conditions, the downregulated genes in the *sir2*-overexpressed mutant represented a small group of all
355 genes induced during infection (Figure 5B, Supplementary Table S7 and Supplementary Table S8).

356 Interestingly, as observed in filamentation conditions (Figure 2F), we detected strong enrichment for
357 genes belonging to the cyan (50%) and the magenta (40%) modules in this group of downregulated
358 genes (Figure 5C, Supplementary Table S7 and Supplementary Table S8). Although Sir2 avoided the
359 full activation of mainly cyan and magenta genes, they were only a small subgroup of the entire
360 modules (19 out of 558 magenta genes showed upregulation in our experiment at 3 dpi, and 26 out of
361 444 total cyan genes) (Supplementary Table S7 and Supplementary Table S8). We wished to determine
362 whether this group of genes has some specific expression profile during infection; therefore, we
363 performed clustering analysis using the expression level of the cyan and magenta gene modules
364 obtained from the RNA-seq data from Lanver *et al.*, 2018 (Lanver et al., 2018). In the resulting
365 heatmap, we marked the Sir2-repressed genes, observing that many of them were clustered together
366 (Figure 5D), indicating that they share a similar expression profile. Specifically, they are genes
367 repressed during the first few days of infection and are strongly induced at 4 dpi, several days after *sir2*
368 overexpression. These data may suggest that the overexpression of *sir2* avoids the subsequent induction
369 of a group of genes induced at 4 dpi, which could explain the decrease in fungal biomass that we
370 observed from this day onwards (Figure 4B). However, it is necessary to exercise caution regarding
371 our timing interpretation, as the data obtained by Lanver *et al*., 2018 (Lanver et al., 2018) were obtained
372 in a different genetic background (FB1xFB2), and the timing of the infection process may not be the
373 same as the one that we observed in an SG200 background, where we conducted the *sir2*
374 overexpression.

375 **Δ*sir2* mutant shows increased acetylation of histone H4 at regulated genes**

376 In order to check whether Sir2 controls filamentation and gene expression through histone
377 deacetylation, we performed Western blot analysis using antibodies against acetylated histone 3 (H3ac)
378 and histone 4 (H4ac), the canonical histone targets of Sir2 (Robyr et al., 2002; Suka et al., 2002;
379 Vaquero et al., 2006; Shimizu et al., 2012; Cai et al., 2021; Zhao and Rusche, 2022), from total proteins
380 extracted after growth in rich media (Figure 6A) and in filamentation induction media (Figure 6B). We
381 did not detect any significant change for these two modifications in either a *sir2* deletion or
382 overexpression mutant (Figures 6A, B). Due to the effect observed in the *sir2* mutants for specific loci
383 rather than broad chromatin regions, we studied the acetylation state of different Sir2 regulated genes.
384 To this aim, we carried out Chromatin Immunoprecipitation (ChIP) experiments using antibodies
385 against H3ac and H4ac followed by RT-qPCR of the promoter region and the ORF of some of the
386 genes that change their expression in the Δ*sir2* mutant in axenic culture (*eff1-9*) (Figure 2C,
387 Supplementary Figure S2.C and Supplementary Table S4), PD-charcoal plates (UMAG_06128, *mig2-*
388 *6*, *rsp3*) (Figure 2D and Supplementary Table S5) and at 3 dpi in the *sir2* overexpressed mutant (*mig2-*
389 *3*, UMAG_01241) (Figure 5A and Supplementary Table S7). As observed in Figure 6C, there was an
390 enrichment of acetylated H4 in *eff1-9* and UMAG_06128 and a slight increase of acetylated H3 in the
391 promoter region of *eff1-9* in the Δ*sir2* mutant. As Sir2 commonly deacetylase lysine 16 in histone 4
392 (H4K16) (Robyr et al., 2002; Suka et al., 2002; Vaquero et al., 2006; Shimizu et al., 2012; Cai et al.,
393 2021; Zhao and Rusche, 2022), we checked the H4K16 acetylation level by ChIP and RT-qPCR of the
394 genes with enriched H4 acetylation, but no differences were observed in the acetylation of this residue
395 (Figure 6D).. Because histone acetylation has been described to be dependent on transcription level
396 (Martin et al., 2021), we checked the reads of the selected target genes obtained in our RNA-seq
397 analysis in axenic condition and observed a correlation between the upregulation of expression on the
398 Δ*sir2* mutant and the increase in acetylation (Figures 6C, E). These data suggest that the increase in
399 histone acetylation is a consequence and not the cause of the gene upregulation and that the defects
400 observed in filamentation and gene regulation in this work are due to a deacetylation-independent
401 function of Sir2 or the deacetylation of a different target.

402 **Discussion**

403 Sirtuins are NAD^+-dependent deacetylases with important regulatory roles in processes such as
404 lifespan, metabolic control or pathogenesis in fungi. As they require the NAD+ cofactor for their
405 activity, sirtuins may serve as regulators of many of these processes in response to metabolic stages.
406 Here, we have performed a systematic analysis of all sirtuins present in *U. maydis* and focused on the
407 nuclear sirtuin Sir2, demonstrating its role in the control of part of the pathogenic program.

408 **The sirtuin repertoire of *U. maydis***

409 Fungal sirtuins can be classified into five principal subfamilies according to their orthologs in other
410 organisms: Sir2/Hst1, Hst2, Hst3/4, SirT4 and SirT5 (Zhao and Rusche, 2022). Interestingly, *U. maydis*
411 harbors a sirtuin member for each subfamily (Elías-Villalobos et al., 2019). The SirT4 and SirT5
412 subfamilies are mitochondrial sirtuins with not many examples described in fungi. We have
413 demonstrated here that the two members of these families in *U. maydis*, Hst5 and Hst6, display
414 mitochondrial localization. However, we have not detected any essential role for them during
415 pathogenesis. On the other hand, Hst2 has been described to show a primary cytoplasmatic localization,
416 although it is involved in locus-specific silencing (Halme et al., 2004; Durand-Dubief et al., 2007) and
417 has a prominent function in chromosome condensation during mitosis (Vaquero et al., 2006; Wilkins
418 et al., 2014; Kruitwagen et al., 2018; Jain et al., 2021). This conflict between location and function
419 may be explained in mammalian cells since Hst2 can move from the cytoplasm to the nucleus, mainly
420 in premitotic cells (Vaquero et al., 2006; Wilson et al., 2006). Similarly to mammalian cells, we have
421 observed that *U. maydis* Hst2 is mainly cytoplasmic, but it is transported to the nucleus in premitotic
422 cells and it remains bound to chromatin during mitosis. This observation strongly supports the idea that
423 in *U. maydis*, Hst2 conserves its role in chromatin condensation during mitosis, probably via the
424 deacetylation of H4K16, as in yeast and mammals (Vaquero et al., 2006; Wilkins et al., 2014). Finally,
425 we found Hst4 and Sir2, members of the Hst3/4 and Sir2/Hst1 subfamilies, respectively, both with
426 constitutive nuclear localization. Although Hst4, as well as the other member of the subfamily, Hst3,
427 may be involved in the transcriptional silencing of a specific locus and heterochromatin (Freeman-
428 Cook et al., 1999; Durand-Dubief et al., 2007), the main function described is their role in chromosome
429 integrity through H3K56 deacetylation. Consequently, cells with a misregulation of these sirtuins show
430 genome stability-related phenotypes such as spontaneous DNA damage, chromosome loss or
431 sensitivity to DNA damage (Celic et al., 2006; Maas et al., 2006; Haldar and Kamakaka, 2008).
432 Although mutants for *hst3* and *hst4* are viable in *S. cerevisiae* and *S. pombe*, the deletion of the single
433 member of this subfamily in *Candida albicans*, *hst3*, which has been demonstrated to be involved in
434 H3K56 deacetylation, has not been possible (Wurtele et al., 2010), suggesting that this gene is essential
435 in this yeast. Here, we have demonstrated that the deletion of *hst4* in *U. maydis* is lethal, which supports
436 again a conserved role of Hst4 in this fungus in genome stability through the acetylation of H3K56.
437 The other nuclear sirtuin in *U. maydis* is Sir2. This is the founding member of the family and has been
438 extensively characterized in different organisms. The main described role for this sirtuin is
439 transcriptional silencing through histone deacetylation, particularly of H4K16 and H3K9 (Robyr et al.,
440 2002; Suka et al., 2002; Vaquero et al., 2006; Shimizu et al., 2012; Cai et al., 2021; Zhao and Rusche,
441 2022). The most recognized biological function for this sirtuin is the regulation of aging (Kaeberlein
442 et al., 1999; Fabrizio et al., 2005; Fu et al., 2008; Bouklas et al., 2017). However, in the human
443 pathogens *Candida glabrata* (Domergue et al., 2005) and *Cryptococcus neoformans* (Arras et al.,
444 2017), in the insect pathogen *Beauveria bassiana* (Cai et al., 2021) and in the plant pathogen
445 *Magnaporthe oryzae* (Fernandez et al., 2014), it has been demonstrated to have implications for the
446 virulence process. In *M. oryzae*, thus far, the only phytopathogen with an in-depth characterization of
447 Sir2, this sirtuin controls virulence through deacetylation of the transcriptional repressor Jmjc, which

448 allows the expression of the superoxide dismutase Sod1, with important roles in ROS detoxification
449 during the first few steps of infection (Fernandez et al., 2014). Here, we provide another example of
450 the role of Sir2 in a phytopathogen, now a basidiomycete, where this sirtuin affects the regulation of a
451 subset of the virulence genes. We have observed that the overexpression of *sir2* reduces the
452 filamentation capability and inhibits the correct induction of virulence genes, affecting proper tumor
453 formation. In contrast, the deletion of *sir2* causes an increase in the filamentation and infection
454 capabilities and allows a better induction of filamentation and virulence genes. Interestingly, Sir2
455 affects filamentation as well in the human pathogen *C. albicans* (Zhao and Rusche, 2021). However,
456 the effect is the reverse, as Sir2 is essential for proper filamentation in this yeast. Further examples of
457 the role of Sir2 in filamentation in different fungi would be useful to verify the possible conserved role
458 of Sir2 during this process.

459 **The role of UmSir2 in transcriptional regulation**

460 Sir2 has a transcriptional silencing role conserved through evolution (Hickman et al., 2011). In high
461 eukaryotes and yeast such as *S. pombe*, with the hallmarks of high eukaryotes and heterochromatin
462 (methylation of H3K9, Heterochromatin Protein 1 (HP1) and RNA interference (RNAi) to produce the
463 heterochromatin silencing platform), Sir2 has been described to aid in the silencing of this region
464 through the deacetylation of histones, mainly H4K16 and H3K9 (Shankaranarayana et al., 2003).
465 However, *U. maydis* lacks all these hallmarks of heterochromatin formation. A similar situation is
466 found in *S. cerevisiae*, where RNAi, H3K9 methylation and HP1 proteins are not present (Hickman et
467 al., 2011). In this organism, Sir2, as part of the SIR complex, together with Sir3 and 4, is the main
468 factor involved in the formation of heterochromatin-like regions (Robyr et al., 2002; Suka et al., 2002).
469 It is tempting to believe that in *U. maydis*, with a similar chromatin scenario, Sir2 would have a similar
470 central role in the silencing of heterochromatin-like regions. However, in *U. maydis*, we did not find
471 homologs of the other members of the SIR complex, which are required for the spreading effect
472 required for heterochromatin formation (Elías-Villalobos et al., 2019). In addition, in a mass
473 spectrometry analysis of a Sir2:eGFP pull down (Supplementary Figure S4), we have not detected any
474 factor belonging to a putative SIR complex. Thus, we observe a different scenario in *U. maydis*, with
475 no hallmarks of heterochromatin and no apparent SIR complex. Our RNA-seq studies reveal that Sir2
476 seems to not be an essential factor for heterochromatin-like silencing in this organism, as we have not
477 found a clear effect in the characteristic heterochromatin regions, such as telomeres or centromeres, or
478 in clusters of coregulated genes, which would be putative chromatin-silenced areas. However, we have
479 found a direct or indirect regulatory effect of Sir2, mainly in silencing, in specific loci. This is
480 consistent with the regulatory effect observed for different sirtuins, including Sir2, and in the general
481 silencing effect observed through evolution (Zhao and Rusche, 2022).

482 An interesting observation is that Sir2 is degraded during filamentation, and we were able to detect
483 two bands of this protein by Western blot (Figure 2A). A tentative speculation is that a posttranslational
484 modification (ptm) of Sir2 during the pathogenic program leads to its degradation and/or inactivation,
485 allowing the proper expression of a pool of virulence genes. Sir2 has been described in yeast to suffer
486 phosphorylation and sumoylation, altering its function (Hannan et al., 2015; Kang et al., 2015). In *M.*
487 *oryzae*, Sir2 accumulation during infection is controlled through ubiquitination by the E3 ubiquitin
488 ligase Upl3, and basal Sir2 levels are controlled by the Grr1 (Patton et al., 1998) and Ptr1 ones (Li et
489 al., 2020). Interestingly, we found UMAG_04611, a homolog of the E3 ubiquitin ligase Skp1, to
490 interact with Sir2 in our mass spectrometry analysis. Further analysis would be interesting to confirm
491 the biological significance of this interaction and the possible role of ubiquitination or other Sir2
492 modifications in *U. maydis* filamentation and virulence.

493 **Possible substrates of Sir2**

494 As mentioned previously, Sir2 represses the transcription of specific substrates or mediates the
495 silencing of heterochromatin regions by the deacetylation of histones, typically H4K16 and H3K9 (25–
496 27, 30, 63, 64). In *U. maydis*, in agreement with the observed repressive effect in specific loci for Sir2,
497 we have not detected any significant change in acetylation for either H3 or H4 by Western blot.
498 However, there is a significant increase of mainly H4 acetylation when specific regulation targets of
499 Sir2 were studied by ChIP and RT-qPCR. Interestingly, we have not observed an increase in acetylation
500 for the specific lysine 16. Although we cannot discard the possibility of a different lysine residue as
501 the target for Sir2, the correlation between the increase in acetylation and the transcriptional
502 upregulation observed, which may indicate an indirect effect in H4 acetylation due to the increase in
503 transcription, suggests a different protein as the target of Sir2 in *U. maydis*. In agreement with this, in
504 the insect pathogen *B. bassiana*, acetylation analysis has revealed that, besides H4 and H3, hundreds
505 of proteins show an altered acetylation pattern in a *sir2* mutant (Cai et al., 2021). More specifically, in
506 plant pathogens, Sir2 has been demonstrated to affect the virulence of *M. orizae* by deacetylation of a
507 transcription factor (Fernandez et al., 2014). In our mass spectrometry analysis, we found the
508 transcription factor Med1 to interact with Sir2 (Supplementary Figure S4). This transcription factor
509 acts upstream of the virulence master regulator Prf1, affecting its expression and virulence (Chacko
510 and Gold, 2012). Although we have not found any significant defect in *prf1* expression on a *sir2*
511 mutant, further investigation would be necessary to study a possible regulatory effect of Sir2 over the
512 Med1 transcription factor and other possible substrates that could explain more in depth the
513 filamentation and transcriptional defects observed on the *sir2* mutant in *U. maydis*.

514 **Funding**

515 This research was supported by MCIN/AEI/10.13039/501100011033/FEDER, grant numbers
516 BIO2016-80180-P and PID2019-110477GB-I00. B.N. was awarded by grant BES-2017-079765
517 MCIN/AEI/FEDER

518 **Author Contributions**

519 RRB and JII designed the concept of the study and supervised the project. BN performed the
520 experiment. RRB and BN analyzed the data. RRB and BN drafted the manuscript. All authors
521 contributed to the article.

522 **Acknowledgements**

523 We thank the Genetics Department for their useful discussions and comments; Víctor Manuel
524 Carranco, Sandra Romero, Laura Tomás and Ismael Fernández Portillo for technical support.

525 **Data availability**

526 RNA sequencing data has been submitted to NCBI Genbank and are available under the following
527 links: httpsXXXXXXXXX

528 **References**

529 Aichinger, C., Hansson, K., Eichhorn, H., Lessing, F., Mannhaupt, G., Mewes, W., et al. (2003).
530 Identification of plant-regulated genes in *Ustilago maydis* by enhancer-trapping mutagenesis.
531 *Mol. Genet. Genomics* 270, 303–314. doi: 10.1007/s00438-003-0926-z.

532 Allfrey, V. G., Faulkner, R., and Mirsky, A. E. (1964). Acetylation and methylation of histones and
533 their role in the regulation of RNA synthesis. *Proc. Natl. Acad. Sci.* 51, 786–794. doi:
534 10.1073/pnas.51.5.786.

535 Arras, S. D. M., Chitty, J. L., Wizrah, M. S. I., Erpf, P. E., Schulz, B. L., Tanurdzic, M., et al. (2017).
536 Sirtuins in the phylum Basidiomycota: A role in virulence in *Cryptococcus neoformans*. *Sci. Rep.*
537 7, 46567. doi: 10.1038/srep46567.

538 Badeaux, A. I., and Shi, Y. (2013). Emerging roles for chromatin as a signal integration and storage
539 platform. *Nat. Rev. Mol. Cell Biol.* 14, 211–224. doi: 10.1038/nrm3545.

540 Becht, P., König, J., and Feldbrügge, M. (2006). The RNA-binding protein Rrm4 is essential for
541 polarity in *Ustilago maydis* and shuttles along microtubules. *J. Cell Sci.* 119, 4964–4973. doi:
542 10.1242/jcs.03287.

543 Bortfeld, M., Auffarth, K., Kahmann, R., and Basse, C. W. (2004). The *Ustilago maydis* a2 mating-
544 type locus genes *lga2* and *rga2* compromise pathogenicity in the absence of the mitochondrial
545 p32 family protein Mrb1. *Plant Cell* 16, 2233–2248. doi: 10.1105/tpc.104.022657.

546 Bouklas, T., Jain, N., and Fries, B. C. (2017). Modulation of replicative lifespan in *Cryptococcus*
547 *neoformans*: Implications for virulence. *Front. Microbiol.* 8. doi: 10.3389/fmicb.2017.00098.

548 Brachmann, A., König, J., Julius, C., and Feldbrügge, M. (2004). A reverse genetic approach for
549 generating gene replacement mutants in *Ustilago maydis*. *Mol. Genet. Genomics* 272, 216–226.
550 doi: 10.1007/s00438-004-1047-z.

551 Brachmann, A., Weinzierl, G., Kamper, J., and Kahmann, R. (2001). Identification of genes in the
552 bW/bE regulatory cascade in *Ustilago maydis*. *Mol. Microbiol.* 42, 1047–1063. doi:
553 10.1046/j.1365-2958.2001.02699.x.

554 Brachmann, C. B., Sherman, J. M., Devine, S. E., Cameron, E. E., Pillus, L., and Boeke, J. D. (1995).
555 The SIR2 gene family, conserved from bacteria to humans, functions in silencing, cell cycle
556 progression, and chromosome stability. *Genes Dev.* 9, 2888–2902. doi: 10.1101/gad.9.23.2888.

557 Brefort, T., Doehlemann, G., Mendoza-Mendoza, A., Reissmann, S., Djamei, A., and Kahmann, R.
558 (2009). *Ustilago maydis* as a Pathogen. *Annu. Rev. Phytopathol.* 47, 423–445. doi:
559 10.1146/annurev-phyto-080508-081923.

560 Brefort, T., Tanaka, S., Neidig, N., Doehlemann, G., Vincon, V., and Kahmann, R. (2014).
561 Characterization of the largest effector gene cluster of *Ustilago maydis*. *PLoS Pathog.* 10,
562 e1003866. doi: 10.1371/journal.ppat.1003866.

563 Cai, Q., Tian, L., Xie, J., Huang, Q., Feng, M., and Keyhani, N. O. (2021). A fungal sirtuin modulates
564 development and virulence in the insect pathogen, *Beauveria bassiana*. *Environ. Microbiol.* 23,
565 5164–5183. doi: 10.1111/1462-2920.15497.

566 Castanheira, S., and Pérez-Martín, J. (2015). Appressorium formation in the corn smut fungus *Ustilago*
567 *maydis* requires a G2 cell cycle arrest. *Plant Signal. Behav.* 10, e1001227. doi:
568 10.1080/15592324.2014.1001227.

569 Celic, I., Masumoto, H., Griffith, W. P., Meluh, P., Cotter, R. J., Boeke, J. D., et al. (2006). The Sirtuins
570 Hst3 and Hst4p preserve genome integrity by controlling histone H3 lysine 56 deacetylation.
571 *Curr. Biol.* 16, 1280–1289. doi: 10.1016/j.cub.2006.06.023.

572 Chacko, N., and Gold, S. (2012). Deletion of the *Ustilago maydis* ortholog of the *Aspergillus*
573 sporulation regulator *medA* affects mating and virulence through pheromone response. *Fungal*
574 *Genet. Biol.* 49, 426–432. doi: 10.1016/j.fgb.2012.04.002.

575 Djamei, A., Schipper, K., Rabe, F., Ghosh, A., Vincon, V., Kahnt, J., et al. (2011). Metabolic priming
576 by a secreted fungal effector. *Nature* 478, 395–398. doi: 10.1038/nature10454.

577 Doehlemann, G., Reissmann, S., Aßmann, D., Fleckenstein, M., and Kahmann, R. (2011). Two linked
578 genes encoding a secreted effector and a membrane protein are essential for *Ustilago maydis*-
579 induced tumour formation. *Mol. Microbiol.* 81, 751–766. doi: 10.1111/j.1365-
580 2958.2011.07728.x.

581 Doehlemann, G., Wahl, R., Vranes, M., de Vries, R. P., Kämper, J., and Kahmann, R. (2008).
582 Establishment of compatibility in the *Ustilago maydis*/maize pathosystem. *J. Plant Physiol.* 165,
583 29–40. doi: 10.1016/j.jplph.2007.05.016.

584 Domergue, R., Castaño, I., De Las Peñas, A., Zupancic, M., Lockatell, V., Hebel, J. R., et al. (2005).
585 Nicotinic acid limitation regulates silencing of *Candida* adhesins during UTI. *Science (80-.).* 308,
586 866–870. doi: 10.1126/science.1108640.

587 Durand-Dubief, M., Sinha, I., Fagerström-Billai, F., Bonilla, C., Wright, A., Grunstein, M., et al.
588 (2007). Specific functions for the fission yeast Sirtuins Hst2 and Hst4 in gene regulation and
589 retrotransposon silencing. *EMBO J.* 26, 2477–2488. doi: 10.1038/sj.emboj.7601690.

590 Elías-Villalobos, A., Barrales, R. R., and Ibeas, J. I. (2019). Chromatin modification factors in plant
591 pathogenic fungi: Insights from *Ustilago maydis*. *Fungal Genet. Biol.* 129, 52–64. doi:
592 10.1016/j.fgb.2019.04.006.

593 Elías-Villalobos, A., Fernández-Álvarez, A., Moreno-Sánchez, I., Helmlinger, D., and Ibeas, J. I.
594 (2015). The Hos2 histone deacetylase controls *Ustilago maydis* virulence through direct
595 regulation of mating-type genes. *PLOS Pathog.* 11, e1005134. doi:
596 10.1371/journal.ppat.1005134.

597 Fabrizio, P., Gattazzo, C., Battistella, L., Wei, M., Cheng, C., McGrew, K., et al. (2005). Sir2 blocks
598 extreme life-span extension. *Cell* 123, 655–667. doi: 10.1016/j.cell.2005.08.042.

599 Farfsing, J. W., Auffarth, K., and Basse, C. W. (2005). Identification of cis -active elements in *Ustilago*
600 *maydis mig2* promoters conferring high-level activity during pathogenic growth in maize. *Mol.*
601 *Plant-Microbe Interact.* 18, 75–87. doi: 10.1094/MPMI-18-0075.

602 Fernandez, J., Marroquin-Guzman, M., Nandakumar, R., Shijo, S., Cornwell, K. M., Li, G., et al.
603 (2014). Plant defence suppression is mediated by a fungal sirtuin during rice infection by
604 *Magnaporthe oryzae*. *Mol. Microbiol.* 94, 70–88. doi: 10.1111/mmi.12743.

605 Freeman-Cook, L. L., Sherman, J. M., Brachmann, C. B., Allshire, R. C., Boeke, J. D., and Pillus, L.
606 (1999). The *Schizosaccharomyces pombe hst4+* gene is a SIR2 homologue with silencing and

607 centromeric functions. *Mol. Biol. Cell* 10, 3171–3186. doi: 10.1091/mbc.10.10.3171.

608 Fu, X.-H., Meng, F.-L., Hu, Y., and Zhou, J.-Q. (2008). *Candida albicans*, a distinctive fungal model
609 for cellular aging study. *Aging Cell* 7, 746–757. doi: 10.1111/j.1474-9726.2008.00424.x.

610 Gillissen, B., Bergemann, J., Sandmann, C., Schroeer, B., Bölker, M., and Kahmann, R. (1992). A two-
611 component regulatory system for self/non-self recognition in *Ustilago maydis*. *Cell* 68, 647–657.
612 doi: 10.1016/0092-8674(92)90141-X.

613 González-Prieto, J. M., Domínguez, A., Rosas-Quijano, R., Cervantes-Chávez, J. A., and Ruiz-
614 Herrera, J. (2004). Isolation and molecular analysis of Umhda2 a gene encoding a histone
615 deacetylase from *Ustilago maydis*. *DNA Seq.* 15, 44–50. doi: 10.1080/10425170310001652192.

616 González-Prieto, J. M., Rosas-Quijano, R., Domínguez, A., and Ruiz-Herrera, J. (2014). The UmGcn5
617 gene encoding histone acetyltransferase from *Ustilago maydis* is involved in dimorphism and
618 virulence. *Fungal Genet. Biol.* 71, 86–95. doi: 10.1016/j.fgb.2014.09.002.

619 Haldar, D., and Kamakaka, R. T. (2008). *Schizosaccharomyces pombe* Hst4 functions in DNA damage
620 response by regulating histone H3 K56 acetylation. *Eukaryot. Cell* 7, 800–813. doi:
621 10.1128/EC.00379-07.

622 Halme, A., Bumgarner, S., Styles, C., and Fink, G. R. (2004). Genetic and epigenetic regulation of the
623 FLO gene family generates cell-surface variation in yeast. *Cell* 116, 405–415. doi:
624 10.1016/S0092-8674(04)00118-7.

625 Hannan, A., Abraham, N. M., Goyal, S., Jamir, I., Priyakumar, U. D., and Mishra, K. (2015).
626 Sumoylation of Sir2 differentially regulates transcriptional silencing in yeast. *Nucleic Acids Res.*
627 43, gkv842. doi: 10.1093/nar/gkv842.

628 Hartmann, H. A., Kahmann, R., and Bölker, M. (1996). The pheromone response factor coordinates
629 filamentous growth and pathogenicity in *Ustilago maydis*. *EMBO J.* 15, 1632–1641. doi:
630 10.1002/j.1460-2075.1996.tb00508.x.

631 Hartmann, H. A., Krüger, J., Lottspeich, F., and Kahmann, R. (1999). Environmental signals
632 controlling sexual development of the corn smut fungus *Ustilago maydis* through the
633 transcriptional regulator Prf1. *Plant Cell* 11, 1293–1305. doi: 10.1105/tpc.11.7.1293.

634 Heimel, K., Scherer, M., Vranes, M., Wahl, R., Pothiratana, C., Schuler, D., et al. (2010). The
635 transcription factor Rbf1 is the master regulator for b-mating type controlled pathogenic
636 development in *Ustilago maydis*. *PLoS Pathog.* 6, e1001035. doi: 10.1371/journal.ppat.1001035.

637 Hickman, M. A., Froyd, C. A., and Rusche, L. N. (2011). Reinventing heterochromatin in budding
638 yeasts: Sir2 and the Origin Recognition Complex take center stage. *Eukaryot. Cell* 10, 1183–1192.
639 doi: 10.1128/EC.05123-11.

640 Itoh, E., Shigemoto, R., Oinuma, K.-I., Shimizu, M., Masuo, S., and Takaya, N. (2017). Sirtuin A
641 regulates secondary metabolite production by *Aspergillus nidulans*. *J. Gen. Appl. Microbiol.* 63,
642 228–235. doi: 10.2323/jgam.2016.11.002.

643 Jackson, M. D., and Denu, J. M. (2002). Structural identification of 2′- and 3′-O-Acetyl-ADP-ribose

644 as novel metabolites derived from the Sir2 family of β-NAD+-dependent histone/protein
645 deacetylases. *J. Biol. Chem.* 277, 18535–18544. doi: 10.1074/jbc.M200671200.

646 Jain, N., Janning, P., and Neumann, H. (2021). 14-3-3 Protein Bmh1 triggers short-range compaction
647 of mitotic chromosomes by recruiting sirtuin deacetylase Hst2. *J. Biol. Chem.* 296, 100078. doi:
648 10.1074/jbc.AC120.014758.

649 Kaeberlein, M., McVey, M., and Guarente, L. (1999). The SIR2/3/4 complex and SIR2 alone promote
650 longevity in *Saccharomyces cerevisiae* by two different mechanisms. *Genes Dev.* 13, 2570–2580.
651 doi: 10.1101/gad.13.19.2570.

652 Kämper, J. (2004). A PCR-based system for highly efficient generation of gene replacement mutants
653 in *Ustilago maydis*. *Mol. Genet. Genomics* 271, 103–110. doi: 10.1007/s00438-003-0962-8.

654 Kämper, J., Kahmann, R., Bölker, M., Ma, L.-J., Brefort, T., Saville, B. J., et al. (2006). Insights from
655 the genome of the biotrophic fungal plant pathogen Ustilago maydis. *Nature* 444, 97–101. doi:
656 10.1038/nature05248.

657 Kang, W. K., Kim, Y. H., Kang, H. A., Kwon, K.-S., and Kim, J.-Y. (2015). Sir2 phosphorylation
658 through cAMP-PKA and CK2 signaling inhibits the lifespan extension activity of Sir2 in yeast.
659 *Elife* 4. doi: 10.7554/eLife.09709.

660 Khrunyk, Y., Münch, K., Schipper, K., Lupas, A. N., and Kahmann, R. (2010). The use of FLP-
661 mediated recombination for the functional analysis of an effector gene family in the biotrophic
662 smut fungus *Ustilago maydis*. *New Phytol.* 187, 957–968. doi: 10.1111/j.1469-
663 8137.2010.03413.x.

664 Kong, X., van Diepeningen, A. D., van der Lee, T. A. J., Waalwijk, C., Xu, J., Xu, J., et al. (2018). The
665 *Fusarium graminearum* histone acetyltransferases are important for morphogenesis, DON
666 biosynthesis, and pathogenicity. *Front. Microbiol.* 9. doi: 10.3389/fmicb.2018.00654.

667 Kruitwagen, T., Chymkowitch, P., Denoth-Lippuner, A., Enserink, J., and Barral, Y. (2018).
668 Centromeres license the mitotic condensation of yeast chromosome arms. *Cell* 175, 780-795.e15.
669 doi: 10.1016/j.cell.2018.09.012.

670 Lanver, D., Berndt, P., Tollot, M., Naik, V., Vranes, M., Warmann, T., et al. (2014). Plant Surface cues
671 prime *Ustilago maydis* for biotrophic development. *PLoS Pathog.* 10, e1004272. doi:
672 10.1371/journal.ppat.1004272.

673 Lanver, D., Müller, A. N., Happel, P., Schweizer, G., Haas, F. B., Franitza, M., et al. (2018). The
674 biotrophic development of *Ustilago maydis* studied by RNA-Seq analysis. *Plant Cell* 30, 300–
675 323. doi: 10.1105/tpc.17.00764.

676 Lanver, D., Tollot, M., Schweizer, G., Lo Presti, L., Reissmann, S., Ma, L.-S., et al. (2017). *Ustilago*
677 *maydis* effectors and their impact on virulence. *Nat. Rev. Microbiol.* 15, 409–421. doi:
678 10.1038/nrmicro.2017.33.

679 Li, G., Qi, X., Sun, G., Rocha, R. O., Segal, L. M., Downey, K. S., et al. (2020). Terminating rice
680 innate immunity induction requires a network of antagonistic and redox-responsive E3 ubiquitin
681 ligases targeting a fungal sirtuin. *New Phytol.* 226, 523–540. doi: 10.1111/nph.16365.

682 Liu, J., An, B., Luo, H., He, C., and Wang, Q. (2022). The histone acetyltransferase FocGCN5 regulates
683 growth, conidiation, and pathogenicity of the banana wilt disease causal agent *Fusarium*
684 *oxysporum f.sp. cubense tropical race 4*. *Res. Microbiol.* 173, 103902. doi:
685 10.1016/j.resmic.2021.103902.

686 Love, M. I., Huber, W., and Anders, S. (2014). Moderated estimation of fold change and dispersion
687 for RNA-seq data with DESeq2. *Genome Biol.* 15, 550. doi: 10.1186/s13059-014-0550-8.

688 Ma, L.-S., Wang, L., Trippel, C., Mendoza-Mendoza, A., Ullmann, S., Moretti, M., et al. (2018). The
689 *Ustilago maydis* repetitive effector Rsp3 blocks the antifungal activity of mannose-binding maize
690 proteins. *Nat. Commun.* 9, 1711. doi: 10.1038/s41467-018-04149-0.

691 Maas, N. L., Miller, K. M., DeFazio, L. G., and Toczyski, D. P. (2006). Cell cycle and checkpoint
692 regulation of histone H3 K56 acetylation by Hst3 and Hst4. *Mol. Cell* 23, 109–119. doi:
693 10.1016/j.molcel.2006.06.006.

694 Martin, B. J. E., Brind'Amour, J., Kuzmin, A., Jensen, K. N., Liu, Z. C., Lorincz, M., et al. (2021).
695 Transcription shapes genome-wide histone acetylation patterns. *Nat. Commun.* 12, 210. doi:
696 10.1038/s41467-020-20543-z.

697 Mazzio, E. A., and Soliman, K. F. A. (2012). Basic concepts of epigenetics. *Epigenetics* 7, 119–130.
698 doi: 10.4161/epi.7.2.18764.

699 Mueller, A. N., Ziemann, S., Treitschke, S., Aßmann, D., and Doehlemann, G. (2013). Compatibility
700 in the *Ustilago maydis*–maize interaction requires inhibition of host cysteine proteases by the
701 fungal effector Pit2. *PLoS Pathog.* 9, e1003177. doi: 10.1371/journal.ppat.1003177.

702 Ökmen, B., Jaeger, E., Schilling, L., Finke, N., Klemd, A., Lee, Y. J., et al. (2022). A conserved enzyme
703 of smut fungi facilitates cell-to-cell extension in the plant bundle sheath. *Nat. Commun.* 13, 6003.
704 doi: 10.1038/s41467-022-33815-7.

705 Patton, El. E., Willems, A. R., and Tyers, M. (1998). Combinatorial control in ubiquitin-dependent
706 proteolysis: don't Skp the F-box hypothesis. *Trends Genet.* 14, 236–243. doi: 10.1016/S0168-
707 9525(98)01473-5.

708 Rando, O. J., and Winston, F. (2012). Chromatin and Transcription in Yeast. *Genetics* 190, 351–387.
709 doi: 10.1534/genetics.111.132266.

710 Reichmann, M., Jamnischek, A., Weinzierl, G., Ladendorf, O., Huber, S., Kahmann, R., et al. (2002).
711 The histone deacetylase Hda1 from *Ustilago maydis* is essential for teliospore development. *Mol.*
712 *Microbiol.* 46, 1169–1182. doi: 10.1046/j.1365-2958.2002.03238.x.

713 Robyr, D., Suka, Y., Xenarios, I., Kurdistani, S. K., Wang, A., Suka, N., et al. (2002). Microarray
714 deacetylation maps determine genome-wide functions for yeast histone deacetylases. *Cell* 109,
715 437–446. doi: 10.1016/S0092-8674(02)00746-8.

716 Ruijter, A. J. M. de, Gennip, A. H. van, Caron, H. N., Kemp, S., and Kuilenburg, A. B. P. van (2003).
717 Histone deacetylases (HDACs): characterization of the classical HDAC family. *Biochem. J.* 370,
718 737–749. doi: 10.1042/bj20021321.

719 Sambrook, J., Frisch, E. R., and Maniatis, T. (1989). *Molecular Cloning: A Laboratory Manual*. 2nd
720 ed. , ed. Cold Spring Harbor NY: Cold Spring Harbor Laboratory Press.

721 Schauwecker, F., Wanner, G., and Kahmann, R. (1995). Filament-specific expression of a cellulase
722 gene in the dimorphic fungus *Ustilago maydis*. *Biol. Chem. Hoppe. Seyler.* 376, 617–626. doi:
723 10.1515/bchm3.1995.376.10.617.

724 Schulz, B., Banuett, F., Dahl, M., Schlesinger, R., Schäfer, W., Martin, T., et al. (1990). The b alleles
725 of *U. maydis*, whose combinations program pathogenic development, code for polypeptides
726 containing a homeodomain-related motif. *Cell* 60, 295–306. doi: 10.1016/0092-8674(90)90744-
727 Y.

728 Schuster, M., Schweizer, G., and Kahmann, R. (2018). Comparative analyses of secreted proteins in
729 plant pathogenic smut fungi and related basidiomycetes. *Fungal Genet. Biol.* 112, 21–30. doi:
730 10.1016/j.fgb.2016.12.003.

731 Shankaranarayana, G. D., Motamedi, M. R., Moazed, D., and Grewal, S. I. S. (2003). Sir2 regulates
732 histone H3 lysine 9 methylation and heterochromatin assembly in fission yeast. *Curr. Biol.* 13,
733 1240–1246. doi: 10.1016/S0960-9822(03)00489-5.

734 Shimizu, M., Masuo, S., Fujita, T., Doi, Y., Kamimura, Y., and Takaya, N. (2012). Hydrolase controls
735 cellular NAD, sirtuin, and secondary metabolites. *Mol. Cell. Biol.* 32, 3743–3755. doi:
736 10.1128/MCB.00032-12.

737 Smith, K. M., Kothe, G. O., Matsen, C. B., Khlafallah, T. K., Adhvaryu, K. K., Hemphill, M., et al.
738 (2008). The fungus *Neurospora crassa* displays telomeric silencing mediated by multiple sirtuins
739 and by methylation of histone H3 lysine 9. *Epigenetics Chromatin* 1, 5. doi: 10.1186/1756-8935-
740 1-5.

741 Suka, N., Luo, K., and Grunstein, M. (2002). Sir2p and Sas2p opposingly regulate acetylation of yeast
742 histone H4 lysine16 and spreading of heterochromatin. *Nat. Genet.* 32, 378–383. doi:
743 10.1038/ng1017.

744 Sutton, A., Heller, R. C., Landry, J., Choy, J. S., Sirko, A., and Sternglanz, R. (2001). A Novel form
745 of transcriptional silencing by Sum1-1 requires Hst1 and the Origin Recognition Complex. *Mol.*
746 *Cell. Biol.* 21, 3514–3522. doi: 10.1128/MCB.21.10.3514-3522.2001.

747 Tanner, K. G., Landry, J., Sternglanz, R., and Denu, J. M. (2000). Silent information regulator 2 family
748 of NAD- dependent histone/protein deacetylases generates a unique product, 1- O- acetyl-ADP-
749 ribose. *Proc. Natl. Acad. Sci.* 97, 14178–14182. doi: 10.1073/pnas.250422697.

750 Tanny, J. C., and Moazed, D. (2001). Coupling of histone deacetylation to NAD breakdown by the
751 yeast silencing protein Sir2: Evidence for acetyl transfer from substrate to an NAD breakdown
752 product. *Proc. Natl. Acad. Sci.* 98, 415–420. doi: 10.1073/pnas.98.2.415.

753 Torreblanca, J., Stumpferl, S., and Basse, C. W. (2003). Histone deacetylase Hda1 acts as repressor of
754 the *Ustilago maydis* biotrophic marker gene *mig1*. *Fungal Genet. Biol.* 38, 22–32. doi:
755 10.1016/S1087-1845(02)00505-4.

756 Vaquero, A., Scher, M. B., Lee, D. H., Sutton, A., Cheng, H.-L., Alt, F. W., et al. (2006). SirT2 is a

757 histone deacetylase with preference for histone H4 Lys 16 during mitosis. *Genes Dev.* 20, 1256–
758 1261. doi: 10.1101/gad.1412706.

759 Vollmeister, E., Schipper, K., Baumann, S., Haag, C., Pohlmann, T., Stock, J., et al. (2012). Fungal
760 development of the plant pathogen *Ustilago maydis*. *FEMS Microbiol. Rev.* 36, 59–77. doi:
761 10.1111/j.1574-6976.2011.00296.x.

762 Wilkins, B. J., Rall, N. A., Ostwal, Y., Kruitwagen, T., Hiragami-Hamada, K., Winkler, M., et al.
763 (2014). A cascade of histone modifications induces chromatin condensation in mitosis. *Science*
764 *(80-.).* 343, 77–80. doi: 10.1126/science.1244508.

765 Wilson, J. M., Le, V. Q., Zimmerman, C., Marmorstein, R., and Pillus, L. (2006). Nuclear export
766 modulates the cytoplasmic Sir2 homologue Hst2. *EMBO Rep.* 7, 1247–1251. doi:
767 10.1038/sj.embor.7400829.

768 Wurtele, H., Tsao, S., Lépine, G., Mullick, A., Tremblay, J., Drogaris, P., et al. (2010). Modulation of
769 histone H3 lysine 56 acetylation as an antifungal therapeutic strategy. *Nat. Med.* 16, 774–780. doi:
770 10.1038/nm.2175.

771 Zhao, G., and Rusche, L. N. (2021). Genetic analysis of sirtuin deacetylases in hyphal growth of
772 *Candida albicans*. *mSphere* 6. doi: 10.1128/mSphere.00053-21.

773 Zhao, G., and Rusche, L. N. (2022). Sirtuins in epigenetic silencing and control of gene expression in
774 model and pathogenic fungi. *Annu. Rev. Microbiol.* 76, 157–178. doi: 10.1146/annurev-micro-
775 041020-100926.

776

777

Figure 1

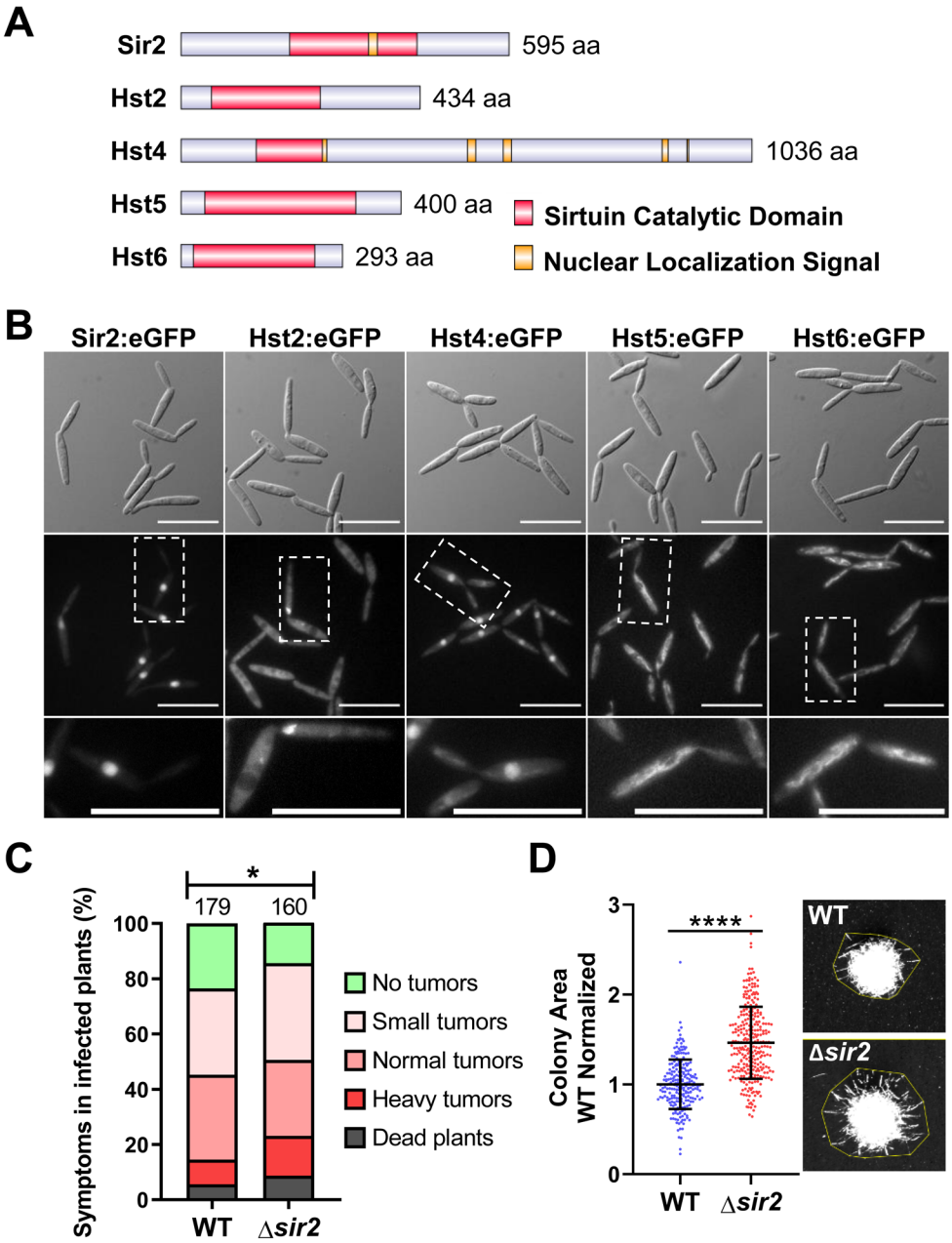
A
Sir2
595 aa
Hst2
434 aa
Hst4
1036 aa
Hst5
400 aa
Hst6
293 aa
Sirtuin Catalytic Domain
Nuclear Localization Signal
B
Sir2:eGFP
Hst2:eGFP
Hst4:eGFP
Hst5:eGFP
Hst6:eGFP
C
Symptoms in infected plants (%)
100
80
60
40
20
0
*
179
160
WT
Δsir2
No tumors
Small tumors
Normal tumors
Heavy tumors
Dead plants
D
Colony Area
WT Normalized
3
2
1
0
****
WT
Δsir2
WT
Δsir2

FIGURE 1. The nuclear sirtuin Sir2 is involved in virulence and filamentation of *Ustilago maydis*. **(A)** Schematic representation of all the sirtuins identified in *U. maydis*. **(B)** Subcellular localization of the indicated *U. maydis* sirtuins tagged with eGFP in its endogenous *loci*. Scale bar represents 20 µm. **(C)** Quantification of symptoms for plants infected with the wild-type and Δ*sir2* mutant at 14 dpi. Total number of infected plants is indicated above each column. Three biological replicates were analyzed. Mann–Whitney statistical test was performed (* p-value < 0.05). **(D)** Quantification of the area of the wild-type and Δ*sir2* mutant single colonies grown on PD–charcoal plates for 48 hours at 25ºC. The colony area was measured as indicated in the stereoscopic images. Data was normalized with the mean of the area of the wild-type colonies. Three biological replicates were analyzed. Student's t-test statistical analysis was performed (**** p-value < 0.001).

Figure 2

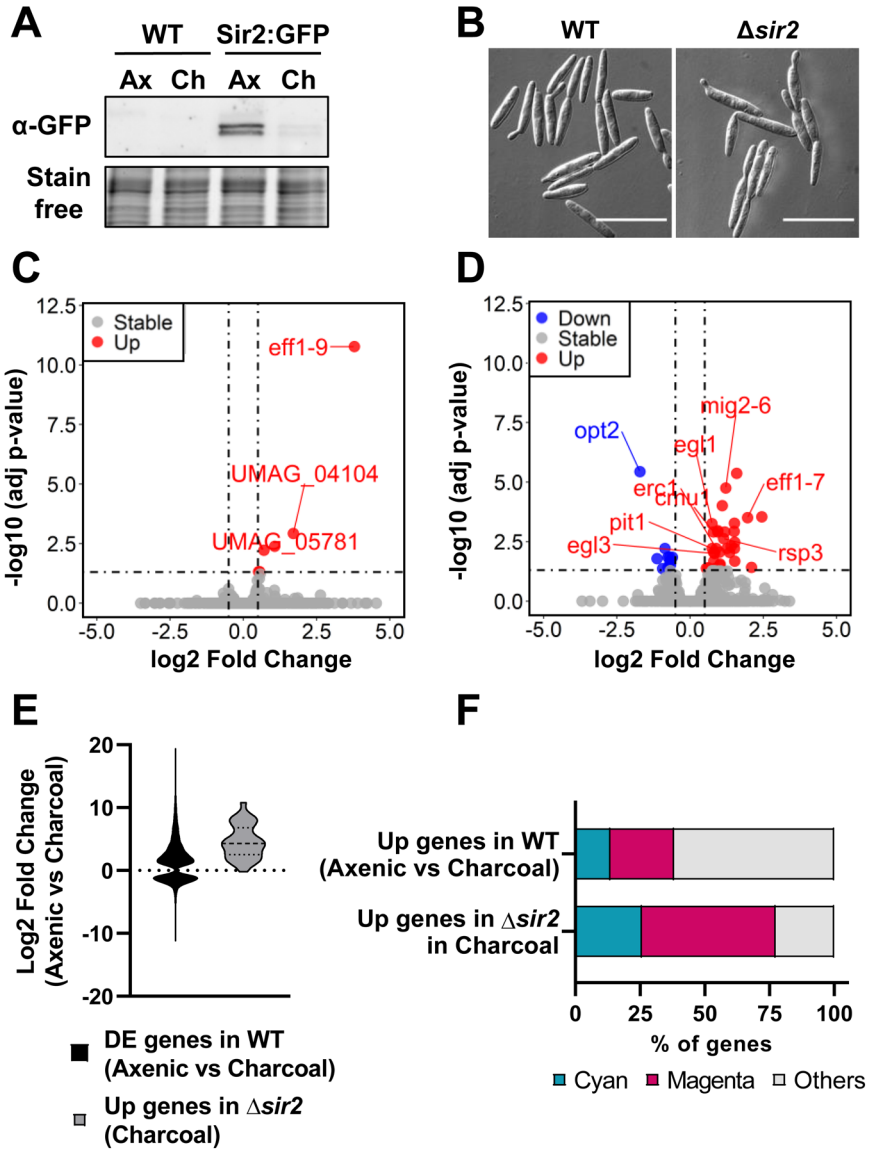
A
WT
Sir2:GFP
Ax
Ch
Ax
Ch
α-GFP
Stain free
B
WT
Δsir2
C
Stable
Up
eff1-9
UMAG_04104
UMAG_05781
-log10 (adj p-value)
log2 Fold Change
D
Down
Stable
Up
opt2
mig2-6
egl1
erc1
cmu1
eff1-7
pit1
egl3
rsp3
-log10 (adj p-value)
log2 Fold Change
E
Log2 Fold Change (Axenic vs Charcoal)
DE genes in WT (Axenic vs Charcoal)
Up genes in Δsir2 (Charcoal)
F
Up genes in WT (Axenic vs Charcoal)
Up genes in Δsir2 in Charcoal
% of genes
Cyan
Magenta
Others

FIGURE 2. Sir2 is degraded during filamentation and is involved in the repression of a group of filamentation-induced genes. **(A)** Western blot showing Sir2:eGFP protein levels of wild-type strain. Total proteins were extracted from cells growing in axenic culture (Ax) and PD–charcoal plates (Ch) for 18 hours at 25ºC. Stain-free gel is shown as a loading control. **(B)** Images of wild-type and Δ*sir2* mutant growing in axenic culture. Scale bar represents 20 µm. **(C, D)** Volcano plot showing the log2 fold change in gene expression and the statistical significance of the differential expression analysis from RNA-seq data obtained for the Δ*sir2* mutant compared to wild-type in axenic culture **(C)** and PD–charcoal plates **(D)**. Red, blue and grey dots represent the upregulated genes (log2 fold change ≥ 0.5, adjusted p-value < 0.05), downregulated genes (log2 fold change ≤ −0.5 adjusted p-value < 0.05) and genes without changes in the Δ*sir2* mutant, respectively. *sir2* data has been removed for plotting purpose. **(E)** Log2 fold change distribution of the differentially expressed genes (adjusted p-value < 0.05) for wild-type in PD–charcoal plates compared to axenic culture (green) and for the upregulated genes in the Δ*sir2* mutant compared to wild-type in PD–charcoal plates (red). **(F)** Percentage of genes belonging to the magenta or cyan modules of coexpressed genes during infection for the upregulated genes of wild-type in PD–charcoal plates compared to axenic culture and for the upregulated genes in the Δ*sir2* mutant compared to wild-type in PD–charcoal plates.

Figure 3

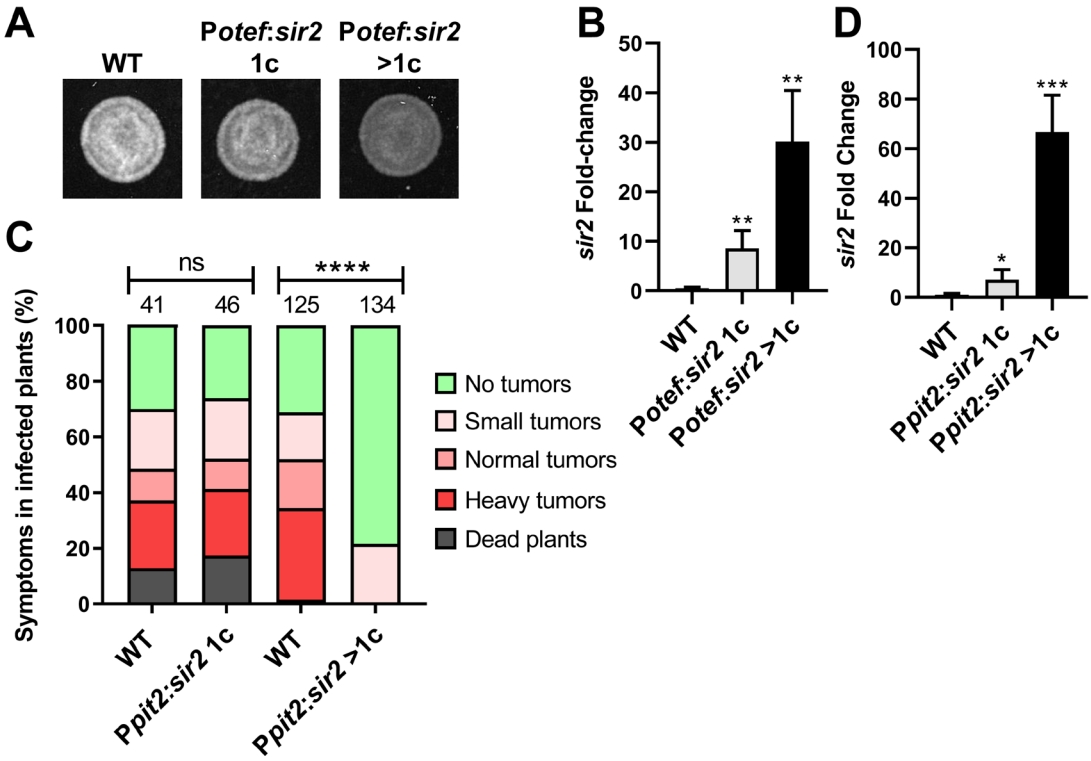
A
WT
Potef:sir2 1c
Potef:sir2 >1c
B
sir2 Fold-change
50
40
30
20
10
0
**
**
WT
Potef:sir2 1c
Potef:sir2 >1c
D
sir2 Fold Change
100
80
60
40
20
0
*
***
WT
Ppit2:sir2 1c
Ppit2:sir2 >1c
C
Symptoms in infected plants (%)
ns
****
41
46
125
134
100
80
60
40
20
0
WT
Ppit2:sir2 1c
WT
Ppit2:sir2 >1c
No tumors
Small tumors
Normal tumors
Heavy tumors
Dead plants

FIGURE 3. Sir2 overexpression reduces filamentation and virulence in *Ustilago maydis*. **(A)** Filamentation of wild-type and *sir2* overexpression mutants containing one (1c) or more copies (>1c) of the P*otef*:*sir2* construct, grown on PD–charcoal plates for 20 hours at 25ºC. **(B)** *sir2* expression levels in axenic culture of wild-type and the *sir2* overexpression mutants measured by RT-qPCR. *U. maydis ppi1* was used as reference gene. Values were normalized to wild-type. Error bars represent the standard deviation from at least three independent replicates. Student's t-test statistical analysis was performed (** p-value < 0.005). **(C)** Quantification of symptoms for plants infected with the indicated strains at 14 dpi. Total number of infected plants is indicated above each column. Three biological replicates were analyzed. Mann–Whitney statistical test was performed (ns, no significant; **** p-value < 0.001). **(D)** *sir2* expression levels of wild-type and the *sir2* overexpression mutants containing one (1c) or more copies (>1c) of the P*pit2*:*sir2* construct infecting maize leaves at 3 dpi, measured by RT-qPCR. *U. maydis ppi1* was used as reference gene. Values were normalized to wild-type. Error bars represent the standard deviation from at least three independent replicates. Student's t-test statistical analysis was performed (** p-value < 0.005).

Figure 4

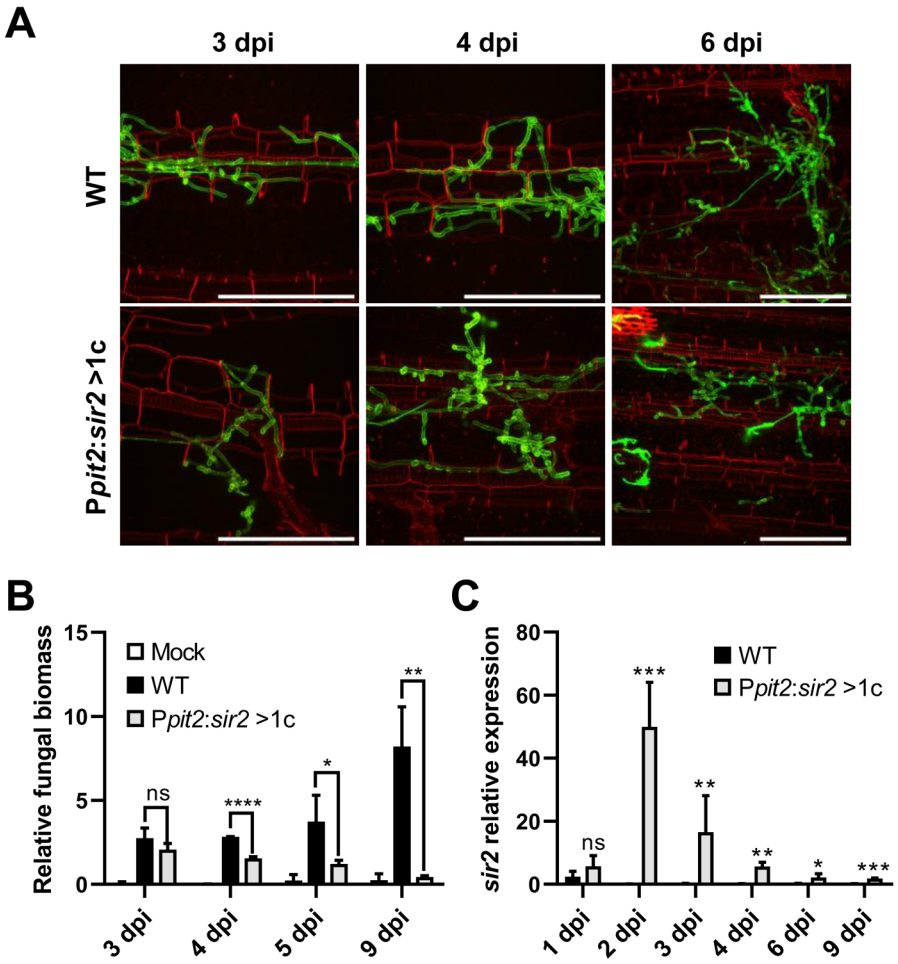
A
3 dpi
4 dpi
6 dpi
WT
Ppit2:sir2 >1c
B
Relative fungal biomass
15
10
5
0
Mock
WT
Ppit2:sir2 >1c
ns
****
*
**
3 dpi
4 dpi
5 dpi
9 dpi
C
sir2 relative expression
80
60
40
20
0
WT
Ppit2:sir2 >1c
ns
***
**
**
*
***
1 dpi
2 dpi
3 dpi
4 dpi
6 dpi
9 dpi

FIGURE 4. Progression inside the plant is impaired by the overexpression of *sir2*. **(A)** Maize leaves from plants infected with wild-type and the P*pit2*:*sir2* >1c mutant at 3, 4 and 6 dpi were stained with propidium iodide (red) and *U. maydis* hyphae with WGA-AF-488 (green) and visualized by fluorescence microscopy. Scale bar represents 100 µm. **(B)** Relative fungal biomass was calculated by comparison between *U. maydis ppi1* gene and *Z. mays* glyceraldehyde 3-phosphate dehydrogenase gene (GAPDH), measured by RT-qPCR of genomic DNA extracted from leaves infected with wild-type and P*pit2*:*sir2* >1c mutant at 3, 4, 5 and 9 dpi. Error bars represent the standard deviation from three independent replicates. Student's t-test statistical analysis was performed (ns, not significant, * p-value <0.05, ** p-value < 0.005, **** p-value < 0.0001). **(C)** *sir2* expression of *U. maydis* wild-type and P*pit2*:*sir2* >1c infecting maize leaves at 1, 2, 3, 4, 6 and 9 dpi, measured by RT-qPCR. *U. maydis ppi1* was used as reference gene. Values were normalized to wild-type. Error bars represent the standard deviation from at least three independent replicates. Student's t-test statistical analysis was performed (ns, not significant, * p-value <0.05, ** p-value < 0.005, *** p-value < 0.0005).

Figure 5

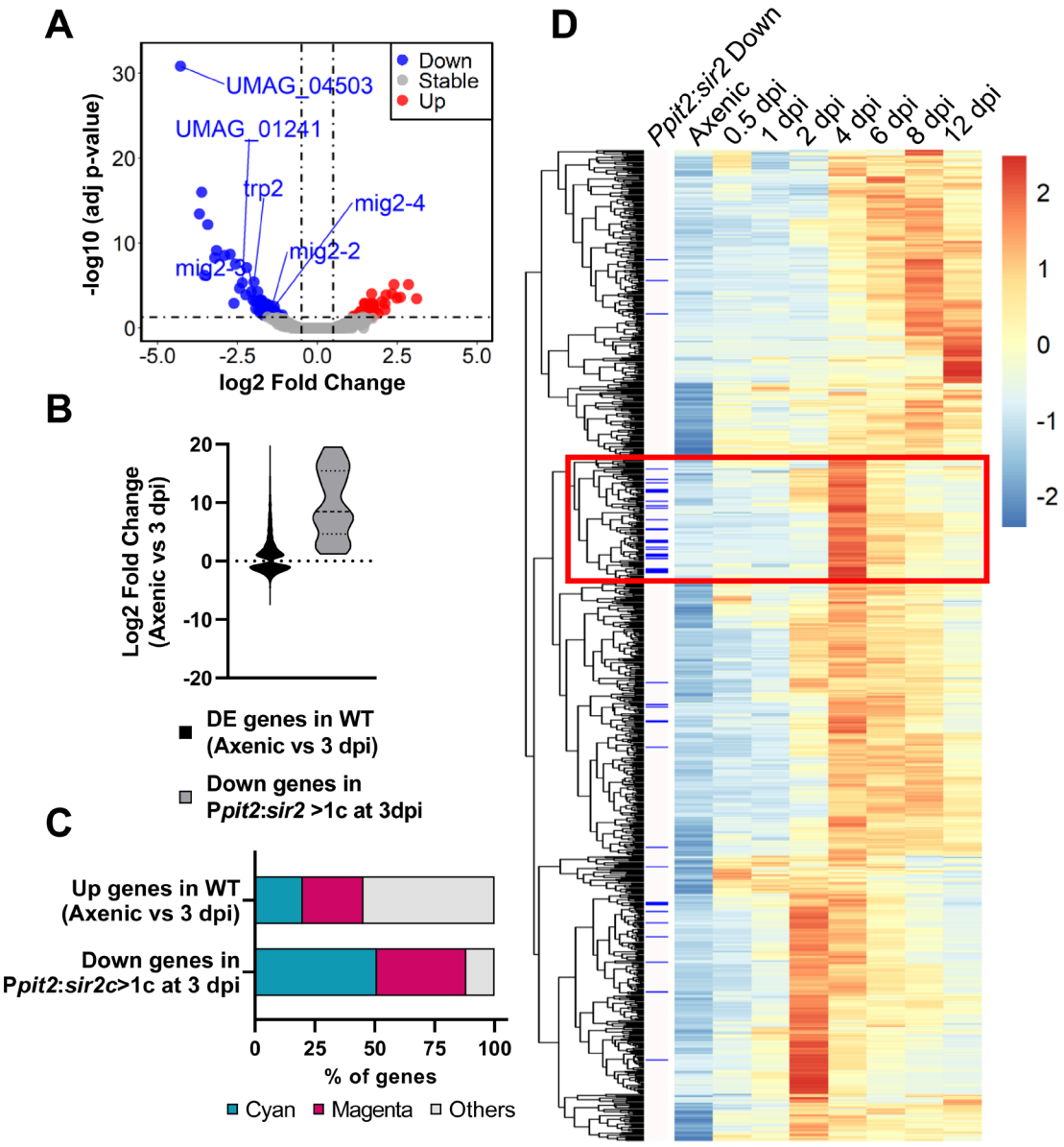
A
Down
Stable
Up
UMAG_04503
UMAG_01241
trp2
mig2-4
mig2-2
mig2-3
-log10 (adj p-value)
log2 Fold Change
B
Log2 Fold Change (Axenic vs 3 dpi)
DE genes in WT (Axenic vs 3 dpi)
Down genes in Ppit2:sir2 >1c at 3dpi
C
Up genes in WT (Axenic vs 3 dpi)
Down genes in Ppit2:sir2c>1c at 3 dpi
% of genes
Cyan
Magenta
Others
D
Ppit2:sir2 Down
Axenic
0.5 dpi
1 dpi
2 dpi
4 dpi
6 dpi
8 dpi
12 dpi

FIGURE 5. Overexpression of *sir2* during pathogenesis avoids the proper activation of a subpopulation of genes related to biotrophism establishment and tumorigenesis. **(A)** Volcano plot showing the log2 fold change in gene expression and the statistical significance of the differential expression analysis from RNA-seq data obtained in the P*pit2*:*sir2* >1c mutant compared to wild-type at 3 dpi. Red, blue and grey dots represent the upregulated genes (log2 fold change ≥ 0.5, adj p-value < 0.05), downregulated genes (log2 fold change ≤ −0.5 adj p-value < 0.05) and genes without changes in the P*pit2*:*sir2* >1c mutant, respectively. *sir2* and *sdh2* (integration resistance cassette used for over expression mutant) data have been removed for plotting purpose. **(B)** Log2 fold change distribution of the differentially expressed genes (adj p-value < 0.05) at 3 dpi compared to axenic conditions in wild-type (green) and the downregulated genes in the P*pit2*:*sir2* >1c mutant compared to wild-type at 3dpi (blue). **(C)** Percentage of genes belonging to the magenta or cyan modules of coexpressed genes during infection for the upregulated genes of wild-type at 3 dpi compared to axenic culture and for the downregulated genes in the P*pit2*:*sir2* >1c mutant compared to wild-type at 3 dpi. **(D)** Clustering analysis of the expression profile of genes belonging to the cyan and magenta modules in axenic cultures and the indicated dpi for the wild-type strain (normalized counts obtained from the published RNA-seq data (Lanver et al., 2018). Heatmap color-scale values correspond to the Z-score transformation of the expression data, with +2 (red) being the highest expression and -2 (blue) being the lowest expression. Blue bars on the left indicate the downregulated genes in the P*pit2*:*sir2* >1c mutant at 3 dpi compared to wild-type.

Figure 6

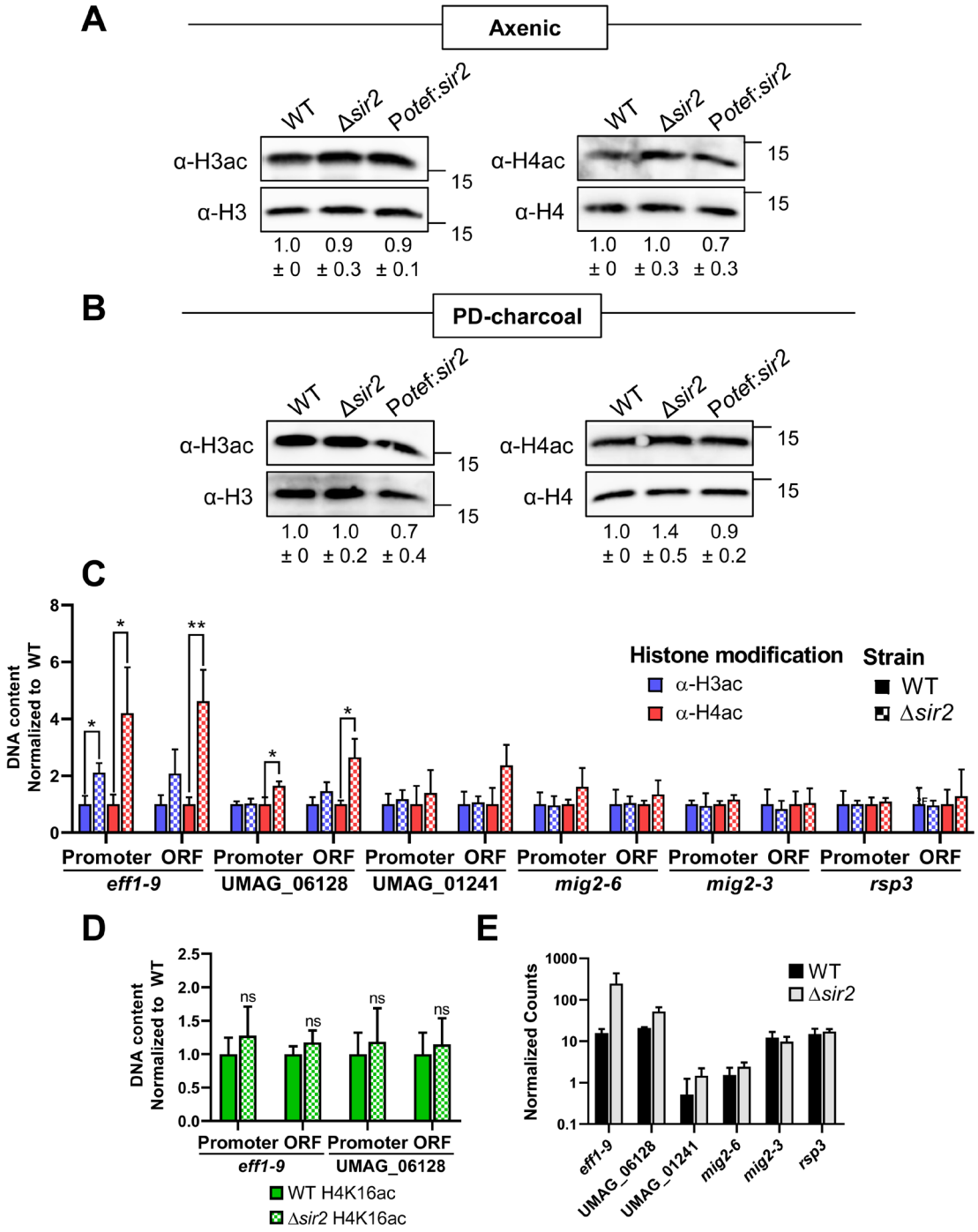
A
Axenic
WT
Δsir2
Potef:sir2
α-H3ac
α-H3
15
15
1.0 ± 0
0.9 ± 0.3
0.9 ± 0.1
α-H4ac
α-H4
15
15
1.0 ± 0
1.0 ± 0.3
0.7 ± 0.3
B
PD-charcoal
WT
Δsir2
Potef:sir2
α-H3ac
α-H3
15
15
1.0 ± 0
1.0 ± 0.2
0.7 ± 0.4
α-H4ac
α-H4
15
15
1.0 ± 0
1.4 ± 0.5
0.9 ± 0.2
C
DNA content Normalized to WT
Histone modification
α-H3ac
α-H4ac
Strain
WT
Δsir2
Promoter ORF
eff1-9
UMAG_06128
UMAG_01241
mig2-6
mig2-3
rsp3
D
DNA content Normalized to WT
ns
Promoter ORF
eff1-9
UMAG_06128
WT H4K16ac
Δsir2 H4K16ac
E
Normalized Counts
WT
Δsir2
eff1-9
UMAG_06128
UMAG_01241
mig2-6
mig2-3
rsp3

FIGURE 6. Effect of *sir2* mutants in histone acetylation. **(A, B)** Total proteins extracted from axenic culture **(A)** or PD-charcoal plates **(B)** of wild-type, Δ*sir2* and the P*otef*:*sir2* >1c strains were used for Western blotting. The H3ac and H4ac antibodies were used to detect histone acetylation and H3 and H4 antibodies were used as loading controls. H3ac and H4ac signals were normalized to H3 and H4 levels, respectively, and compared to wild-type from three independent replicates. **(C, D)** ChIP analysis using H3ac and H4ac antibodies **(C)** or H4K16ac antibody **(D)** on chromatin extracts from axenic culture of wild-type and Δ*sir2* strains. Immunoprecipitated DNA was analyzed by RT-qPCR, amplifying regions within the promoter and the open reading frame (ORF) of the indicated gene. Values correspond to the amount of DNA recovered in the IP relative to *ppi1* gene. Values were normalized to wild-type. Error bars represent the standard deviation from at least three independent replicates. Student's t-test statistical analysis was performed (ns, no significant, * p-value <0.05, ** p-value < 0.005). **(E)** Mean of the normalized count of the indicated genes obtained in the RNA-seq experiment in the wild-type and Δ*sir2* strains in axenic condition.